Multi-omic analysis of the Arabidopsis clock activator mutant *rve 4 6 8* reveals connections to carbohydrate metabolism and proteasome regulation

Scandola S[1*], Mehta D[1*], Li Q[1], Rodriguez M[1], Castillo B[1], and Uhrig RG[1,#]

Department of Biological Sciences, University of Alberta, Edmonton, AB, Canada

[#]Corresponding Author
R. Glen Uhrig
Department of Biological Sciences
University of Alberta
11455 Saskatchewan Drive
Edmonton, Alberta
Canada
T6G 2E9
* denotes equal authorship

Keywords: Circadian Clock, *Arabidopsis thaliana*, Quantitative Proteomics, Phosphoproteomics, Metabolomics,

Running Title: RVE4, 6 and 8 induce multifaceted protein-level changes

ABSTRACT

Plants are able to sense changes in their light environments, such as the onset of day and night, as well as anticipate these changes in order to adapt and survive. Central to this ability is the plant circadian clock, a molecular circuit that precisely orchestrates plant cell processes over the course of a day. REVEILLE proteins (RVEs) are recently discovered members of the plant circadian circuitry that activate the evening complex and PRR genes to maintain regular circadian oscillation. The RVE 8 protein and its two homologs, RVE 4 and 6, have been shown to limit the length of the circadian period, with *rve 4 6 8* triple-knockout plants possessing an elongated period along with increased leaf surface area, biomass, cell size and delayed flowering relative to wild-type Col-0 plants. Here, using a multi-omics approach consisting of phenomics, transcriptomics, proteomics, and metabolomics we draw novel connections between RVE8-like proteins and a number of core plant cell processes. In particular, we reveal that loss of RVE8-like proteins results in altered carbohydrate, organic acid and lipid metabolism, including a starch excess phenotype at dawn. We further demonstrate that *rve 4 6 8* plants have lower levels of 20S proteasome subunits and possess significantly reduced proteasome activity, potentially explaining the increase in cell-size observed in RVE8-like mutants. Overall, this robust, multi-omic dataset, provides substantial new insights into the far reaching impact RVE8-like proteins have on the diel plant cell environment.

INTRODUCTION

The circadian clock is a central regulator of plant growth and development that modulates plant responses to both internal and external cues (Greenham and McClung, 2015; Nohales and Kay, 2016; McClung, 2019). It is comprised of a number of transcription factors that function as a series of interlocking molecular circuits that precisely time the 24-hour photoperiod (Creux and Harmer, 2019). Correspondingly, knockout mutants of circadian clock transcription factors have been extensively studied at the phenotypic, genetic and transcript-level in the model plant *Arabidopsis thaliana* (Creux and Harmer, 2019; McClung, 2019; Nakamichi, 2020), with upwards of 30% of genes shown to be under circadian control (Covington et al., 2008). This extensive body of work has revealed a number of roles for the circadian clock in plants, including in the timing of flowering (Shim et al., 2017), disease resistance (Lu et al., 2017) and mitigation of abiotic stress (Simon et al., 2020; Kidokoro et al., 2021) amongst others. However, despite the extensive use of genetic and transcriptomic technologies to understand the molecular impacts of core circadian clock components in *Arabidopsis*, much less is known about how, and/or if, these transcriptional changes manifest at the protein-level (Choudhary et al., 2015; Choudhary et al., 2016; Krahmer et al., 2022; Uhrig et al., 2019; Mehta et al., 2021; Uhrig et al., 2021).

Protein abundance and post-translational protein modification (PTM) changes are critical control mechanisms for biological systems. To date, quantitative proteomic analysis of circadian clock mutants *lhy cca1*, *prr7 prr9*, *gi* and *toc1* at end-of-day (ED; ZT12) and end-of-night (EN; ZT0) time-points (Graf et al., 2017) and time-course experimentation involving $CCA1_{ox}$ (Krahmer et al., 2022) and wild-type (WT) Col-0 (Uhrig et al., 2021) plants over free-running and 12:12 light:dark (LD) conditions have provided the first insights into where diel changes in the proteome manifest. Similarly, time-course and ED versus EN analyses of the phosphoproteome from $CCA1_{ox}$ (Krahmer et al., 2022) and WT Col-0 (Uhrig et al., 2019) plants point to a critical, but largely unexplored, role for protein phosphorylation and other PTMs in diel plant cell regulation; particularly at ED and EN. Beyond proteomics, quantitative metabolomic analyses of core circadian clock mutants can also help define the role the circadian clock plays in regulating growth and

84 development through the modulation of primary metabolism (Fukushima et al., 2009; Flis
85 et al., 2019).
86 REVEILLE (RVE) genes are recently discovered additions to the circadian clock that
87 have been found to function as core circadian clock activators, modulating the regulation
88 of the evening complex (EARLY FLOWERING 3 (ELF3), 4 (ELF4) and LUX
89 ARRHYTHMO (LUX)) in addition to TIMING OF CAB EXPRESSION 1 (TOC1) and
90 PSEUDO RESPONSE REGULATOR 5 (PRR5) (Farinas and Mas, 2011; Rawat et al.,
91 2011; Hsu et al., 2013; Gray et al., 2017). Findings that *rve 8* (Farinas and Mas, 2011;
92 Rawat et al., 2011) and *rve 4 6 8* (Gray et al., 2017) plants possess an elongated circadian
93 period demonstrate how RVE proteins are important to maintaining the pace of the
94 circadian clock, while phenotypic characterization of the *rve 4 6 8* plants revealed greater
95 plant growth and cell size, coupled with a delay in flowering (Gray et al., 2017).
96 Despite these findings, how RVE8-like proteins regulate the diel plant cell environment
97 at the protein- and metabolic-level remains unresolved. To address this gap in knowledge,
98 we have undertaken a multi-omic analysis of *rve 4 6 8* plants relative to WT Col-0 at
99 critical diel / circadian time-points; EN / ZT0 and ED / ZT12. Here, we demonstrate that
100 loss of RVE 4, 6 and 8 results in extensive diel proteome, phosphoproteome and
101 metabolome changes spanning a wide array of critical plant cell processes. In particular,
102 our results suggest that RVE8-like proteins impact critical elements of primary metabolism
103 such as transient diel leaf-starch / carbohydrate levels. Perhaps most intriguingly, we find
104 that *rve 4 6 8* plants maintain extensive protein- and PTM-level perturbations in
105 proteasome subunits, coupled with reduced proteasome activity and altered amino acids
106 levels, which together, likely form the basis of the increased growth phenotype of *rve 4 6*
107 *8*. As RVE8-like proteins are associated with multiple agronomically important traits such
108 as biomass and flowering time, elucidating their role in modulating the diel proteome,
109 PTMome and metabolome is critical for their potential implementation in crop
110 improvement strategies.
111
112 **RESULTS**
113 **Examination of *rve 4 6 8* mutant phenotypes reveals starch excess at dawn.**

114 In order to ensure our molecular analysis would provide robust results, we first
115 phenotypically characterized *rve 4 6 8* plants relative to WT Col-0 (Col-0) under our
116 growth conditions (12:12 LD photoperiod facilitated by LED lights). Here, we were able to
117 reproduce multiple growth and development phenotypes previously observed (Gray et
118 al., 2017), indicating that our growth conditions are comparable (Supplemental Figure 1).
119 We monitored plant area and perimeter using real-time imaging over 5 days and found
120 significant differences between *rve 4 6 8* and WT Col-0 arise by day 17 post-imbibition,
121 with *rve 4 6 8* plants possessing increased leaf area and perimeter (Supplemental Figure
122 1A & B). We then performed fresh and dry weight measurements of *rve 4 6 8* versus WT
123 Col-0 plants at day 19 post-imbibition revealing that *rve 4 6 8* has greater biomass
124 (Supplemental Figure 1C & D). Lastly, under our 12:12 LD conditions, we found *rve 4 6*
125 *8* plants have delayed flowering relative to WT Col-0 (Supplemental Figure 1E).
126 Given these growth phenotypes and the previously observed response of *rve 4 6 8* to
127 sucrose (Gray et al., 2017), we next stained *rve 4 6 8* and WT Col-0 rosettes for the
128 accumulation of transient leaf starch over a 12:12 LD photoperiod examining ZT0, 6, 12
129 and 18 time-points. This revealed that *rve 4 6 8* plants possess a starch excess phenotype
130 at ZT0 (Figure 1A). We then validated this analysis by performing an enzymatic
131 quantitation of starch levels in WT Col-0 and *rve 4 6 8* plants (Figure 1B). Samples were
132 collected hourly from ZT21 to ZT3 in order to enzymatically assess if the starch excess
133 observed was due to the long-period phase shift of the *rve 4 6 8* mutant clock. Here, our
134 results indicate that the observed starch excess is in fact independent of the long-period
135 phase shift of the *rve 4 6 8* mutant (Figure 1B). We then further examined three key starch
136 metabolism related enzymes for changes in their gene expression using NanoString RNA
137 quantification: *PHOSPHOGLYCERATE MUTASE 1* (*PGM1*), *GRANUAL BOUND*
138 *STARCH SYNTHASE 1* (*GBSS1*) and *STARCH EXCESS 4* (*SEX4*). *GBSS1* and *SEX4*
139 transcript levels were significantly lower in *rve 4 6 8* compared to WT Col-0 at ZT0 and
140 ZT12, respectively, while no change was observed in PGM expression (Figure 1C and
141 D). Together with our phenotypic data, these results suggest a potential disconnect
142 between the timing of starch degradation and biosynthesis that results in greater transient
143 starch accumulation at dawn.
144

145 **Gene expression analysis provides molecular insights into *rve 4 6 8* growth**
146 **phenotypes.**

147 Using NanoString RNA quantification, we next examined the expression of a panel of
148 core circadian clock genes and genes involved in processes impacted by the circadian
149 clock (Figure 2; Supplemental Figure 2 Supplemental Data 1). Studies examining RVE 8-
150 like proteins (RVE 4, 6 & 8) have observed changes in multiple core circadian clock and
151 clock-associated genes (Creux and Harmer, 2019), including *PSEUDO RESPONSE*
152 *REGULATOR 5* (*PRR5*), *TIMING OF CAB1 EXPRESSION 1* (*TOC1*), *EARLY*
153 *FLOWERING 4* (*ELF4*), *PHYTOCHROME INTERACTING FACTOR 4* (*PIF4*) and *5*
154 (*PIF5*). We aimed to consolidate this understanding by examining changes in these
155 genes, amongst others, in *rve 4 6 8* plants at ZT0 and ZT12 time-points under 12:12 LD
156 conditions. Here, we find a decrease in *TOC1* and *ELF4* transcript levels combined with
157 an increase in *PRR5*, *PIF4* and *PIF5* expression in *rve 4 6 8* at ZT12 (Figure 2A). We also
158 observed a decrease in *CIRCADIAN CLOCK REGULATED 1* (*CCA1*) and *LATE*
159 *ELONGATED HYPOCOTYL* (*LHY*) expression at ZT0 along with increases in *PSEUDO*
160 *RESPONSE REGULATOR 7* (*PRR7*) and *GIGANTEA* (*GI*) at ZT12 that are also
161 consistent with an elongated period (Hsu et al., 2013; Flis et al., 2016). While our PRR5
162 result accords with previous findings, our Nanostring quantification shows reduced TOC1
163 transcript levels while previous qPCR results have shown increased TOC1 levels at ZT12
164 (Hsu et al, 2013). Similarly, while we observe reduced transcript levels of LHY and CCA1
165 in the mutant, the previous study does not observe any difference. These differences
166 between the two studies is likely due to the different measurement techniques used
167 (qPCR vs Nanostring) and the relatively larger variation in expression recorded in Hsu et
168 al. 2013. Collectively, our results align with previous research examining RVE8-like
169 proteins, however, more time-points are needed to precisely define the impact of RVE8-
170 like proteins on the phasing and period lengths of core clock transcripts.

171 Photoreceptors are crucial in circadian clock entrainment by light, but are in turn also
172 controlled by the clock (Bognar et al., 1999; Sanchez et al., 2020). Correspondingly, we
173 next examined *rve 4 6 8* plants for changes in the expression of key photoreceptor genes,
174 quantifying changes in the expression of *PHYTOCHROME* (*PHY*) *A* and *B*,
175 *PHOTOTROPIN* (*PHOT*) *1* and *2*, *CRYPTOCHROME 1* (*CRY1*) and the circadian clock

176 associated photoreceptor *ZEITLUPE* (*ZTL*) in *rve 4 6 8* versus WT Col-0 at ZT0 and ZT12.
177 Here, we found a significant decrease in *PHYA* and a significant increase in *PHOT1*
178 expression in *rve 4 6 8* plants at ZT12, with no change in *PHYB*, *PHOT2*, *CRY1* and *ZTL*
179 (Figure 2B).
180 Since *rve 4 6 8* plants demonstrate a number of growth phenotypes, we additionally
181 examined the expression of genes upstream of, or involved in, phytohormone related-
182 processes. Here, we find significant changes in *GERANYLGERANYL*
183 *PYROPHOSPHATE SYNTHASE 1* (*GGPPS1*) at both ZT0 and ZT12 as well
184 *ARABIDOPSIS RESPONSE REGULATOR 7* (*ARR7*) at ZT12 (Supplemental Figure 2).
185 While these genes represent only a sampling of the phytohormone metabolism / signaling
186 landscape, both their enzyme products have a common connection to Dimethylallyl
187 Pyrophosphate (DMAPP) / Isoprenyl Pyrophosphate (IPP), a critical metabolic
188 intermediate. GGPPS1 catalyzes the entry point reaction for downstream production of
189 multiple phytohormones, including: abscisic acid, gibberellin and stringolactone
190 biosynthesis (Ruiz-Sola et al., 2016). Cytokinin is also derived from the DMAPP / IPP
191 metabolic branch point (Astot et al., 2000) and ARR7 represents a cytokinin response
192 factor that is activated in the presence of cytokinins (Huang et al., 2017).
193
194 **Quantitative proteome and phosphoproteome analyses reveal extensive protein-**
195 **level impacts of RVE8-like protein loss.**
196 Quantifying proteome-level changes in the plant cell environment in response to
197 perturbation (e.g. gene deletion) is a robust means of measuring the impact of a protein
198 on a system. However, the high dynamic range nature of plant tissues has typically
199 hampered our ability to sufficiently sample the dynamically fluctuating proteome, biasing
200 analyses towards high abundant proteins (Mehta et al., 2022; Mehta et al., 2021). Given
201 this, we deployed a combination of BoxCarDIA (proteome abundance) and conventional
202 DDA (phosphoproteomics) mass spectrometry acquisition methods to perform label-free
203 quantitation (LFQ) of protein abundance and phosphoproteomic changes in *rve 4 6 8*
204 plants at ZT0 and ZT12. The ZT0 and ZT12 time-points were selected for analysis as they
205 have been shown to exhibit dynamic protein-level changes (e.g. abundance and PTMs)
206 across multiple plant organs, tissues and growth conditions in a variety of wild-type and

207 circadian clock mutant plants (Graf et al., 2017; Krahmer et al., 2022; Uhrig et al., 2019;
208 Uhrig et al., 2021). Through this analysis we quantified 3,934 proteins and 1,137
209 phosphoproteins for changes in abundance and phosphorylation status, of which 536 and
210 346 demonstrated significant fluctuations, respectively (Table I; Supplemental Data 2 and
211 3). Further, we quantified 46% of all proteins exhibiting a significant change in their
212 phosphorylation status at the proteome-level (159 / 347 phosphoproteins), with 8.6% of
213 phosphoproteins demonstrating a corresponding change in protein abundance (30 / 347
214 phosphoproteins).

215 Next, using significantly changing proteins and phosphoproteins, we performed a
216 gene ontology (GO) enrichment analysis for biological processes, subcellular localization
217 and molecular function to reveal how the loss of RVE8-like proteins impacts the diel plant
218 cell environment at the protein-level (Figure 3; Supplemental Data 4). Here, we found
219 changes in 'proteolysis' (GO:0006508), which was complemented by the enrichment of
220 'proteasome core complex' (GO:0005839) and 'proteasome complex' (GO:0000502)
221 subcellular localizations, in addition to 'response to acid chemical' (GO:0001101), which
222 represents a high-level category for phytohormones and 'polysaccharide metabolism'
223 (GO:0005976), amongst others (Figure 3A). Similarly, phosphoproteomic data revealed
224 enrichment in 'response to acid chemical' (GO:0001101) and 'response to abscisic acid'
225 (GO:0009737) in addition to 'cell cycle' (GO:0007049), 'cell division' (GO:0051301),
226 'macromolecule metabolism' (GO:0043170) and 'response to lipids (GO:0033993),
227 amongst others (Figure 3B). While proteome-level *rve 4 6 8*-dependent changes included
228 both increases and decreases in protein levels, we found a global increase in protein
229 phosphorylation in the *rve 4 6 8* mutant compared to WT Col-0 (Figure 3B).

230 Lastly, we compared our significantly changing phosphopeptides at ZT0 and ZT12
231 with phospho-sites previously found to oscillate under free-running conditions in WT Col-
232 0 (Krahmer et al., 2022). Here we found that 77 of our phosphopeptides (*q-value* ≤ 0.05)
233 significantly changed in *rve 4 6 8* compared to WT Col-0 (JTK *p-value* ≤ 0.05;
234 Supplemental Data 5). These oscillating phosphopeptides are from diverse, but critically
235 important proteins such as nuclear localized RETINOBLASTOMA-RELATED 1 (RBR;
236 AT3G12280) – growth and development, cytosolic PHOSPHOENOLPYRUVATE
237 CARBOXYLASE 2 (PEPC2; AT2G42600) and chloroplast-targeted RUBISCO

238 ACTIVASE (AT2G39730) - metabolism and plasma membrane associated CELLULOSE
239 SYNTHASE-LIKE D3 (CSLD3; AT3G03050) – cell wall biosynthesis (Supplemental Data
240 5). This indicates that RVE8-like proteins influence the timing of diel phosphorylation
241 events on proteins involved in core growth and development processes.
242
243 **Time-of-day association network analysis finds multiple gene networks affected in**
244 ***rve 4 6 8* at the protein-level.**
245 To contextualize the changing proteome and phosphoproteome, we next generated
246 STRING-DB association networks (minimum edge score ≥ 0.7) for all significantly
247 changing proteins and phosphoproteins in *rve 4 6 8* plants at ZT0 and ZT12 relative to
248 WT Col-0 to better understand the protein-level changes that underpin observed *rve 4 6*
249 *8* phenotypes. Proteome quantification revealed decreases in the abundance of multiple
250 starch degradation enzymes including STARCH EXCESS 1 (SEX1; AT1G10760) and
251 SEX4 as well as cold-stress proteins COLD-REGULATED 15A (COR15A; AT2G42540),
252 15B (COR15B; AT2G42530) and 6 (COR6; AT5G15970). Conversely, we observed
253 increases in primary metabolic and sulfur assimilation enzymes such as
254 PHOSPHOFRUCTOKINASE 5 (PFK5; AT2G22480), PYRUVATE ORHOPHOSPHATE
255 DIKINASE (PPDK; AT4G15530) 5'-ADENYLYLPHOSPHOSULFATE REDUCTASE 2
256 (APR2; AT1G62180) and ADENYLYL-SULFATE KINASE (APK; AT2G14750), along with
257 a multitude of spliceosomal, ribosomal and ubiquitin ligating proteins. Together, these
258 proteomic data support our observed starch excess phenotype in *rve 4 6 8* at ZT0, while
259 suggesting RVE8-like proteins also impact agronomically important processes such as
260 sulfur assimilation and cold stress response (Figure 4). We also observed distinct
261 changes in proteasome complex proteins, whereby four 19S proteasome proteins
262 (AT1G04810, AT1G75990; AT4G19006, AT4G24820) are up-regulated and twelve 20S
263 proteasome proteins are down-regulated in *rve 4 6 8* plants (Figure 4; Supplemental Data
264 6). Further examination of the transcripts corresponding to the proteasome subunits
265 changing at the protein-level using DiurnalDB (http://diurnal.mocklerlab.org/) found that 9
266 of the 12 20S subunits and 2 of the 4 19S subunits possess daily oscillations in their
267 transcripts (≥ 0.8 cutoff), with most peaking in abundance at ZT12 (Supplemental Data
268 6).

269 Association network analysis also revealed that the loss of RVE8-like proteins results
270 in major phosphoproteome perturbations, with large increases in the phosphorylation
271 status of a number of proteins at both ZT0 and ZT12 in *rve 4 6 8* (Figure 5).
272 Correspondingly, we observed abundance changes in protein kinases (PKs) CALCIUM
273 DEPENDENT PROTEIN KINASE 3 (CDPK6/CPK3; AT4G23650), 29 (CPK29;
274 AT1G76040), CYTOPLASMIC TRNA EXPORT PROTEIN (CTEXP; AT2G40730), WALL
275 ASSOCIATED KINASE 1 (WAK1; AT1G21250), amongst others (Figure 4), in addition to
276 phosphorylation changes on 23 protein kinase superfamily proteins including CPK1
277 (Figure 5). Overall, we observed phosphorylation changes on proteins involved in similar
278 processes and protein complexes as those found in our quantitative proteome data
279 including multiple spliceosomal- and ribosome- complex proteins, ubiquitin-related
280 proteins and primary metabolic enzymes (Figure 5). Exclusive to our phosphoproteome
281 data however, are perturbations in the phosphorylation status of a number of nuclear-
282 and secretion-related proteins along with extensive changes in proteins related to light
283 harvesting, photosynthesis and light signaling, such as CAB1 (AT1G29930), PHOT2
284 (AT5G58140) and HY5 (AT5G11260).
285 Next, we performed a phospho-motif enrichment analysis using our significantly
286 changing phosphopeptides to identify potential PKs regulated by RVE8-like proteins. We
287 found 5 enriched phosphorylation motifs relating to MITOGEN ACTIVATED PROTEIN
288 KINASES (MAPKs), CASEIN KINASE II (CKII) and CALCIUM DEPENDENT PROTEIN
289 KINASES (CDPK/CPKs) (Supplemental Data 7). Using the phosphoproteins containing
290 these motifs, we then created a STRING-DB association network (minimum edge score
291 ≥ 0.7) depicting the phosphorylated substrates of these PKs found in our study to resolve
292 potential functional relationships as well as intersections between different PKs
293 (Supplemental Figure 3). Again, a stringent minimum edge score was used to resolve
294 robust network connections, however here, all phosphoproteins recognized as having one
295 of these 5 motifs is shown. This analysis resolved a number of networks, including: 26S
296 proteasomal complex proteins - MAPK, ribosome - CKII / CDPK/CPK, spliceosome -
297 CDPK/CPK, RNA processing - MAPK and golgi-ER secretion - CDPK/CPK relationships
298 (Supplemental Figure 3), collectively providing new cell signaling – biological process
299 connections for further characterization.

300

301 **Wide ranging primary metabolite changes highlight altered metabolism in *rve 4 6 8***
302 **plants.**

303 As multiple proteins involved in metabolism demonstrated changes at the proteome
304 and phosphoproteome level, we next examined diel changes in *rve 4 6 8* metabolism
305 compared to WT Col-0 at ZT0, 6, 12 and 18 using gas chromatography mass
306 spectrometry (Figure 6; Supplemental Data 8). Here, we found dynamic changes (*rve 4*
307 *6 8* vs. WT Col-0) in amino acids (AA), organic acids (OA), fatty acids (FA) and sugars,
308 amongst others, over the course of the day, with the largest perturbations occurring
309 around ZT0 - ZT6. These diel changes are highlighted by large increases in phenylalanine
310 (AA), glutamic acid (AA), shikimic acid (OA), sinapinic acid (OA), α-linolenic acid (FA),
311 sucrose (sugar), myo-inositol (other), 5-oxoproline (other) and phytol (other) at ZT0, along
312 with an increase in mannose (sugar) staring at ZT6. Further, we observe that *rve 4 6 8*
313 plants maintain a consistent increase in glyceric acid (OA) and fumaric acid (OA) coupled
314 with a consistent decrease in serine (AA) and threonine (AA) across all four ZT time-
315 points harvested.

316

317 ***rve 4 6 8* plants possess constitutively reduced proteasome activity**

318 The enrichment of proteolysis and proteasome related GO categories in our
319 proteomics dataset, coupled with an extensive cluster of proteasome-related proteins in
320 our STRING-DB association network, prompted us to examine whether the *rve 4 6 8*
321 mutant showed differences in proteasome function compared to WT Col-0. We therefore
322 carried out a proteasome activity assay using a 7-Amino-4-methylcoumarin (AMC)
323 flurophore tagged LLVY peptide substrate (Üstün et al., 2017) and used the well
324 characterized MG132 proteasome inhibitor as a negative control to validate the assay.
325 Proteasome activity was measured in crude extracts of 8 independent wild-type and *rve*
326 *4 6 8* rosettes harvested at both ZT23 and ZT11. Our results show a significant reduction
327 in proteasome activity in the *rve 4 6 8* mutant compared to wild-type (adjusted *p-value* ≤
328 0.05; Bonferroni & Dunn multiple testing correction) (Figure 7A). Further, plants with
329 impaired proteasome activity are also found to display a hypersensitivity to chemical
330 proteasome inhibition (Gladman et al., 2016; Han et al., 2019). Correspondingly, when

331 grown on plates containing 50μM of the MG132 proteasome inhibitor, *rve 4 6 8* seedlings
332 possessed impaired growth, similar to that previously observed in mutants of both the
333 core 20S proteasome and the NAC transcription factors that activate the proteasome
334 stress regulon (Figure 7B, Supplemental Figure 4) (Gladman et al., 2016; Han et al.,
335 2019).
336
337 **DISCUSSION**
338 **Multi-omics analysis reveals altered carbohydrate metabolism in *rve 4 6 8* plants**
339 Through our combined use of phenomics, transcriptomics, proteomics and
340 metabolomics, we found that *rve 4 6 8* plants possess a starch excess phenotype at ZT0
341 that relates to altered both gene expression and protein abundance changes in starch
342 biosynthesis and degradation enzymes. Initial examination of the transcriptional changes
343 of select genes saw significant decreases in *GBSS1* at ZT0 and *SEX4* at ZT12 in *rve 4 6*
344 *8* relative to WT Col-0, respectively. Subsequent proteomic analysis then found extensive
345 decreases in nearly all facets of the starch degradation machinery at either ZT0 and/or
346 ZT12 including decreases in the abundance of SEX1 (AT1G10760), SEX4, GWD3
347 (AT5G26570), ISA3 (AT4G09020), PHS2 (AT3G46970), LDA (AT5G04360) and DPE2
348 (AT2G40840) (Streb and Zeeman, 2012). Correspondingly, our metabolite data
349 demonstrated decreased glucose and sucrose levels at ZT6, ZT12 and ZT18, which is
350 consistent with altered carbon metabolism related to excess starch levels at ZT0. Plants
351 deficient in core clock proteins PRR7 and PRR9 (*prr7 prr9*), which also maintain a long
352 circadian period, have also been shown to possess a subtle starch excess phenotype
353 (Chew et al., 2017; Flis et al., 2019); however, unlike *prr7 prr9* plants, *rve 4 6 8* plants
354 seem to asymmetrically possess excess starch at ZT0 only. The mutant of
355 disproportionating enzyme (DPE1; AT5G64860), a key starch degradation protein,
356 however, possesses a similar phenotype whereby starch levels are in excess at dawn but
357 accumulate closer to wild-type plants by dusk (Critchley et al, 2001). We also see DPE1
358 asymmetrically down-regulated in protein abundance at ZT0, suggesting a connection to
359 RVE8-like proteins. Hence, future work connecting RVE8-like proteins to DPE1 and other
360 starch degradation enzymes is certainly of interest.

361 Interestingly, we see very few PTM-level changes occurring on starch-related
362 enzymes in *rve 4 6 8* plants despite many of these enzymes being previously found to be
363 phosphorylated (PhosPhat; http://phosphat.uni-hohenheim.de/; (Heazlewood et al.,
364 2008)). Unlike the extensive protein abundance changes observed, only two starch-
365 related enzymes were found to have a significant change in their phosphorylation status.
366 These were STARCH SYNTHASE 2 (SS2; AT3G01180) and BETA-AMYLASE 1 (BAM1;
367 AT3G23920), of which both exhibited an increase in their phosphorylation status at ZT0
368 and ZT12 in *rve 4 6 8* relative to WT Col-0. The role(s) of protein phosphorylation in
369 regulating starch-related enzyme complexes has been well defined in sink tissues (Tetlow
370 et al., 2004), but remains poorly understood in source tissues (e.g. leaves), where starch
371 is produced and degraded on a daily basis (Smith and Zeeman, 2020). Recent
372 biochemical characterization of SS2 phosphorylation using phospho-ablative SS2
373 mutants (S63A and S65A) found no enzymatic or protein complex consequences to the
374 loss of SS2 phosphorylation despite being phosphorylated by CKII; (Patterson et al.,
375 2018)). Our data finds SS2 to be phosphorylated at Ser65; part of a canonical CKII
376 phosphorylation motif (*pS*[D/E][D/E][D/E]) (Purzner et al., 2018), exclusively at ZT0 in the
377 *rve 4 6 8* mutant. We also observe BAM1 to be phosphorylated, but at a *pS*P MAPK-like
378 motif (Purzner et al., 2018). There are no currently defined roles for BAM1
379 phosphorylation despite its key role in regulating plant growth, promoting stomatal
380 opening and facilitating starch degradation under osmotic stress in the light (Thalmann et
381 al., 2016).
382 Of the carbohydrate-related changes we found in *rve 4 6 8*, the consistent and
383 substantial increase in mannose, a multifunctional glucose analog, was particularly
384 interesting. Previous investigations of the function of mannose have found that it can: 1)
385 stimulate stomatal closure (Hei et al., 2018), 2) be incorporated into glycolysis through
386 fructose 6-phosphate via hexokinase and phosphomannose isomerase (Sharma et al.,
387 2014), 3) protect against oxidative damage, 4) impact flowering time through ascorbate
388 production (Kotchoni et al., 2009) and 5) contribute to cell wall biosynthesis and protein
389 glycosylation (Qi et al., 2017) - all molecular changes that relate to the phenotypes
390 displayed by *rve 4 6 8*. Interestingly, mannose has a high affinity for hexokinase (Herold
391 and Lewis, 1977), leading to the induction of glucose-like signaling responses such as

392 stomatal closure (Hei et al., 2018) and bud elongation in *Arabidopsis*, pea and rose
393 (Barbier et al., 2021). It is possible that a similar mechanism contributes to the elongated
394 rosette leaf morphology observed in *rve 4 6 8,* both in this study, and others (Gray et al.,
395 2017).
396
397 **RVE8-like protein regulation of TOC1 may control the production of fumarate and**
398 **other organic acids**
399 *Arabidopsis* plants over-expressing RVE8 have previously been shown to stimulate
400 the expression of *TOC1* (Hsu et al., 2013) and *toc1-2* plants have been found to possess
401 increased levels of fumarate at ZT7 and Z19 (Cervela-Cardona et al., 2021). In this
402 context, our finding that *rve 4 6 8* plants possess both reduced *TOC1* gene expression at
403 ZT12 and increased fumarate levels throughout the diel cycle, suggests RVE8-like
404 proteins impact fumarate metabolism via TOC1. Further, this finding aligns with our
405 observation that multiple other mitochondrial organic acids are, to varying degrees,
406 impacted by RVE8-like proteins, including malate, citrate and succinate. Change in these
407 organic acids align with the previous findings that *prr5 prr7 prr9* mutants have increased
408 fumarate, malate, citrate and succinate stemming from the down-regulation of TCA-cycle
409 genes (Fukushima et al., 2009). At the protein-level however, we find no significant
410 change in FUMARASE 1 (FUM1; AT2G47510), FUMARASE 2 (FUM2; AT5G50950),
411 MITOCHONDRIAL MALATE DEHYDROGENASE 1 (mMDH1; AT1G53240), mMDH2
412 (AT3G15020), CITRATE SYNTHASE 2 (CSY2; AT3G58750), CSY3 (AT2G42790),
413 SUCCINATE DEHYDROGENASE 1-1 (SDH1-1; AT5G66760), SDH5 (AT1G47420) and
414 SDH6 (AT1G08480) protein abundance and/or PTM levels in *rve 4 6 8* versus WT Col-0
415 at either ZT0 or ZT12. This indicates that RVE8-like protein control of fumarate production
416 is not direct, but likely through the previously identified TOC1-FUM2 mechanism (Cervela-
417 Cardona et al., 2021). It also suggests that if diel protein-level regulation of mitochondrial
418 TCA enzymes is occurring, it manifests through alternative means, such as a production-
419 degradation mechanism that maintains steady state levels of TCA enzymes or through
420 PTMs other than phosphorylation. While our current dataset is unable to directly answer
421 these possibilities, previous work examining mitochondrial protein turnover has implicated
422 FTSH, LON and CLPXP proteases (Li et al., 2017; Huang et al., 2020), of which we

423 observe FTSH11 (AT5G53170) and CLPX (AT5G53350), two putatively mitochondrial
424 targeted proteases, to possess an increase in their phosphorylation status (Heazlewood
425 et al., 2004; Senkler et al., 2017). Ultimately how TCA enzymes are coordinately
426 regulated at the transcript, protein and/or PTM-levels, in addition to possible feed-forward
427 or feed-back regulation by metabolites, requires targeted analyses that are beyond the
428 scope of this study.
429
430 **RVE8-like proteins are constitutive regulators of the proteasome**
431 Both GO enrichment and STRING-DB association network analysis of differentially
432 expressed proteins in *rve 4 6 8* at ZT0 and ZT12 revealed substantial protein-level
433 changes in the abundance of a number of proteasome complex subunits, coupled with a
434 limited corresponding change in phosphorylation status. In plants, connections between
435 the circadian clock and E3 ubiquitin ligases targeting proteins for proteasomal
436 degradation through K63 polyubiquitylation have emerged, indicating that diel protein
437 turnover is a circadian controlled phenomenon (Feke et al., 2019; Feke et al., 2020; Zhu
438 et al., 2020a). Further, using N^{15} labeling methods, efforts made to quantify protein
439 turnover rates have demonstrated that diel protein turnover involves a multitude of
440 proteins that are processed at variable rates over a wide-ranging time frame (Li et al.,
441 2017; Huang et al., 2020). To date however, no connections between the circadian clock
442 and the direct regulation of the proteasome complex have been uncovered.
443 The mature 26S proteasome is comprised of a 20S core protease (CP) which
444 maintains non-specific ubiquitin-independent proteolytic activity and 19S regulatory
445 particle (RP) subunits that determine specificity to ubiquitylated proteins (Sadanandom et
446 al., 2012). We observe a reduction in 12 out of the 14 CP subunits, including 5 alpha and
447 7 beta ring subunits, in the *rve 4 6 8* mutants. In contrast, we see an increase in the
448 abundance of 4 RP subunits, as well as CSN4, a member of the COP9 signalosome, a
449 conserved regulator of ubiquitin-dependent proteolysis and a key player in
450 photomorphogenesis (Qin et al., 2020). Studies investigating proteasome subunits in
451 Arabidopsis have shown that reduced CP proteolytic function is associated with cell
452 expansion (Kurepa et al., 2009a) and that one member of the 19S RP subunit, RPN12a,
453 is involved in cytokinin-mediated signaling for cell division (Smalle et al., 2002). This

454 aligns with our GO enrichment of cell cycle and cell division biological process amongst
455 proteins exhibiting a significant change in abundance as well as our observed increase in
456 cytokinin response factor ARR7. Further, these findings are consistent with a hypothesis
457 that proper balancing of the 20S and 19S subunits of the proteasome is key for
458 maintaining growth and cell division (Kurepa et al., 2009b), and that alterations in the
459 levels of these subunits in *rve 4 6 8*, at least partially, explain its growth and large cell size
460 phenotypes.

461 In mice, connections between the circadian clock and proteasomal degradation of
462 CRYPTOCHROME 1 (CRY1) have also been defined, with enhanced CRY1 degradation
463 associated with elevated glucose levels and a loss of core clock regulation (Toledo et al.,
464 2018). In plants, CRY proteins entrain the clock (Devlin and Kay, 2000), with *cry1* mutants
465 having longer circadian periods under blue light (Somers et al., 1998). Interestingly, in *rve*
466 *4 6 8* plants, which similarly possess a long circadian period that increases with blue light
467 fluence (Gray et al., 2017), we observe increased CRY1 protein levels at both ZT0
468 (Log_2FC = 1.05) and ZT12 (Log_2FC = 0.81), coupled with a starch excess phenotype and
469 wide-ranging carbohydrate metabolism perturbations, indicating a potentially similar
470 circadian clock intersection between CRY1 and primary carbohydrate metabolism that
471 appears to involve RVE8-like proteins. Additionally, the diel amino acid perturbations
472 measured in *rve 4 6 8* plants may also correspond to RVE8-like proteins impacting the
473 diel plant cell environment through the regulation of proteasome subunits and protein
474 turnover.

475 Ultimately, a connection between the circadian clock and diel protein turnover is
476 logical given the consistent lack of coordinately fluctuating diel transcripts and proteins in
477 *Arabidopsis* across multiple experiments (Baerenfaller et al., 2012; Graf et al., 2017;
478 Mehta et al., 2021; Uhrig et al., 2021). Overall, our results implicate RVE8-like proteins
479 as being involved in diel protein turnover, adding important context to the well-known
480 disconnect between circadian transcript and protein abundancies. Future assessment of
481 core circadian clock mutants for changes in protein turnover rates may help resolve the
482 degree to which diel protein turnover contributes to daily protein-level plant cell regulation.
483

484 **Proteome changes in *rve 4 6 8* plants suggest RVE8-like proteins may modulate**
485 **adaptive plant stress responses**

486 The enrichment of GO categories pertaining to Abscisic acid in the *rve 4 6 8* proteome,
487 provides protein-level evidence that RVE8-like proteins may modulate adaptation to
488 drought-like stresses (e.g. osmotic, salinity, and cold). A potential role for RVE8-like
489 proteins in drought-like stress response(s) is supported by the measured increase in
490 mannose-levels, which is known to influence stomatal conductance. Further, α-linolenic
491 acid, and its derivatives, are known to increase upon drought and salinity stress to
492 mitigate associated cell membrane issues by remodeling cell membranes to increase
493 their fluidity (Zhang et al., 2005; Upchurch, 2008; Torres-Franklin et al., 2009; He and
494 Ding, 2020). Here, this seems to center on FATTY ACID DESATURASE 7 (FAD7;
495 AT3G11170), which utilizes linoleic acid to produce α-linolenic acid (Gibson et al., 1994),
496 and is significantly more abundant in *rve 4 6 8* plants at ZT0, corresponding to peak levels
497 of α-linolenic acid.

498 In addition to augmenting membrane fluidity, α-linolenic acid can also fuel the
499 production of jasmonic acid (JA) (He and Ding, 2020). Interestingly, we find that critical
500 jasmonic acid biosynthetic enzymes AOC1, AOC2 and 12-OXOPHYTODIENOATE
501 REDUCTASE 3 (OPR3; AT2G06050) are significantly more abundant in WT Col-0
502 relative to *rve 4 6 8*, suggesting that RVE8-like protein deficient plants may possess
503 susceptibility to certain biotic stresses. A diel connection between RVE8-like proteins and
504 JA biosynthetic enzymes is further supported by the altered diel phosphorylation of the
505 peroxisomal ABC transporter COMATOSE (CTS; AT4G39850), which imports JA
506 precursor *cis*-12-oxophytodienoic acid that is then utilized by OPR3 (Wasternack and
507 Hause, 2019), which peaks in protein abundance at ZT12.

508 Further support for a role of RVE8-like proteins in drought-like stress response(s) is
509 the increased abundance of key sulfur assimilating enzymes APR2 (AT1G62180) and
510 APK (AT2G14750) in *rve 4 6 8* plants. These proteins are critical for the production of
511 ABA and glutathione (GSH), in addition to a number of other critical plant metabolites
512 (Aarabi et al., 2020). Correspondingly, we see an increase in a number of glutathione
513 transferases (GSTs); GSTF2, GSTF6 (AT1G02930) and GSTF7 (AT1G02920), which are
514 a subclass of the plant-specific Phi-family of GSTs implicated in mitigating oxidative

515 (GSTF2) and salt (GSTF6/7) stress, respectively (Lee et al., 2014; Seok et al., 2020). In
516 previous proteomic and phosphoproteomic analyses of persistent osmotic and salt-
517 stress, increased abundance of sulfur metabolic enzymes (Rodriguez et al., 2021),
518 indicates a potential connection between sulfur metabolism / assimilation and drought-
519 stress tolerance. In maize, the application of sulfur-supplemented fertilizers to drought
520 stressed plants was shown to mitigate the effects of drought (Usmani et al., 2020).
521 RVE8-like proteins were most recently implicated in the direct transcriptional activation
522 of DEHYDRATION RESPONSE ELEMENT B (DREB) expression under cold-stress
523 (Kidokoro et al., 2021). DREB transcription factors serve as master controllers of cold-
524 induced gene expression, regulating COLD REGULATED (COR) genes to enhance
525 freezing tolerance (Jaglo-Ottosen et al., 1998). Correspondingly, RVE8-like protein
526 deficient plants (*rve 4 8*) possessed diminished cold tolerance (Kidokoro et al., 2021).
527 Interestingly, our proteomics data resolved a cluster of cold-stress related proteins that
528 are reduced in abundance at ZT12 / ED under normal growth temperatures, suggesting
529 that some cold response proteins are diel regulated, likely possessing additional diel roles
530 beyond cold-stress response (Maszkowska et al., 2018; Zhu et al., 2020b). These include:
531 chloroplast targeted COR15A (AT2G42540) and COR15B (AT2G42530) (Artus et al.,
532 1996) as well as cytoplasmic-targeted KIN2/COR6.6 (AT5G15970), ERD10
533 (AT1G20450), AT1G54410 and AT4G30650. In conjunction with our analyses, these
534 findings directly connect RVE8-like proteins to observable proteome-level changes in
535 genes associated with drought-related stresses.
536
537 **Protein kinases impacted by RVE8-like proteins**
538 In addition to catalyzing the phosphorylation of target proteins, protein kinases (PKs)
539 themselves are often phosphorylated, resulting in changes in their activity, function or
540 localization, forming a complex signaling web that can have far-reaching ramifications for
541 plant cell function. Our combined quantitative proteomic and phosphoproteomic analysis
542 uncovered a number of PKs that change in either diel abundance or phosphorylation
543 status in response to the loss of RVE8-like proteins. Of particular interest is the increased
544 abundance of CASEIN KINASE II (CKIIα; AT2G23070), CALCIUM DEPENDENT
545 PROTEIN KINASE 6 (CDPK6/CPK3; AT4G23650) and WALL ASSOCIATED KINASE 1

546 (WAK1; AT1G21250) and the phosphorylation of CPK1 (AT5G04870), as these PKs have
547 been implicated in multiple plant cell processes related to *rve 4 6 8* phenotypes as well
548 as osmotic- and salt-stress tolerance.

549 CKII is a well-known clock associated kinase that directly affects the stability of core
550 clock component CCA1 in *Arabidopsis* (Sugano et al., 1998; Lu et al., 2011). The role of
551 CKII in modulating the circadian clock is conserved across eukaryotes, with both
552 mammalian (Tamaru et al., 2009) and Drosophila (Akten et al., 2003) circadian clocks
553 being directly impacted by CKII. Most recently, multiple CASEIN KINASE 1 family kinases
554 were discovered to phosphorylate PRR5 and TOC1 leading to their degradation (Uehara
555 et al., 2019). Our finding that CKII levels are elevated in *rve 4 6 8* at ZT12 hints at the
556 possibility of RVE8-like proteins similarly directing CKII-mediated phospho-regulation of
557 circadian function. Beyond the clock, CKII has been implicated in phosphorylating
558 numerous light signaling proteins, such as HY5 (Hardtke et al., 2002), which we see here
559 possessing an increase in its phosphorylation status in *rve 4 6 8* plants at Ser36 at both
560 ZT0 and ZT12. Recently, HY5 phosphorylation at Ser36 was found to be phosphorylated
561 by SUPPRESSOR OF PHYTOCHROME A-105 (SPA) kinases (Wang et al., 2021),
562 suggesting that perhaps other CKII-motif containing proteins resolved here may also
563 represent SPA targets. Lastly, CKII is also characterized as phosphorylating ABA / abiotic
564 stress induced pathway proteins (Mulekar and Huq, 2014), which aligns with our
565 enrichment of ABA-related GO terms in our phosphoproteomic data.

566 CDPK6/CPK3 is a positive regulator of ABA-induced regulation of stomatal closure
567 (Mori et al., 2006) and is induced under high salt conditions (Mehlmer et al., 2010),
568 suggesting that its increased abundance in *rve 4 6 8* plants may convey signaling events
569 related to osmotic- / salt-stress response. Although CDPK6/CPK3 has not been shown to
570 directly impact the circadian clock, its connection to stomatal regulation, coupled with
571 known diel fluctuations in calcium levels (Marti Ruiz et al., 2020), suggests a connection
572 to the regulation of diel plant cell processes. Similar to CDPK6/CPK3 salt-stress induction,
573 over-expression of native CPK1 resulted in increased salinity tolerance in cell culture
574 (Veremeichik et al., 2021), reinforcing a potential link between diel CPK-mediated
575 phosphorylation events and the ability to mitigate abiotic stress. Alternatively, WAK1 has
576 been implicated in maintaining cell wall integrity (Leschevin et al., 2021), which has diel

577 plant cell growth implications that may contribute to the large mesophyll cell phenotype
578 of *rve 4 6 8* plants (Gray et al., 2017).
579 These results, when combined with our phospho-motif analysis that shows an
580 enrichment in CKII and CDPK/CPK target motifs, suggest that CKIIα and CDPK6/CPK3
581 may be connected to a substantial portion of the observed RVE8-like dependent
582 phosphoproteome. STRING-DB association network analysis of proteins with these
583 enriched phospho-motifs demonstrates connections to multiple nuclear protein networks
584 including one involving RETINOBLASTOMA-RELATED 1 (RBR; AT3G12280), a critical
585 growth and development protein, in addition to protein translation and secretion.
586 Collectively, these data provide novel insights into RVE8-like protein dependent phospho-
587 networks and the corresponding kinases that may be involved.
588
589 **CONCLUSION**
590 Our robust, multi-omic analysis of *rve 4 6 8* plants further establishes RVE8-like
591 proteins as targets of agronomic interest by defining the proteomic and metabolic
592 underpinnings of their observable phenotypes. Through these analyses, we found a
593 number of connections to clock related cell processes that refine our understanding of *rve*
594 *4 6 8* growth phenotypes. This includes altered metabolism that either directly (e.g.
595 carbohydrates and organic acids) or indirectly (e.g. precursors for growth phytohormones)
596 drives growth outcomes. In particular, carbohydrate metabolism, for which we found a
597 significant decrease in multiple starch degradation enzymes leading to starch excess at
598 dawn. As well, our findings reveal that RVE8-like proteins control the 26S proteasome
599 through altered 20S and 19S subunit abundance and phosphorylation status, which our
600 metabolite data suggests may be tied to changes in resource pools important for growth
601 and development (e.g. amino acids). This novel connection between the proteasome and
602 the circadian clock through RVE8-like proteins was further supported by a reduction of
603 proteasome activity in *rve 4 6 8* plants, something that in proteasome mutants, leads to a
604 large cell size phenotype similar to that observed in *rve 4 6 8* plants. This suggests that
605 RVE8-like proteins regulate the proteasome as a means of controlling cell division and
606 growth. Lastly, our multi-omic analyses hint at potential new connections between RVE8-
607 like proteins and abiotic stress response (e.g. osmotic, salt and/or cold – already

608 established), which we see manifesting throughout our proteome, phosphoproteome and
609 metabolome data. Overall, our combined use of quantitative transcriptomics, proteomics,
610 PTMomics and metabolomics have elucidated a number of new connections between
611 RVE8-like proteins and critical plant cell processes, laying a substantial foundation from
612 which to build a comprehensive understanding of the roles RVE8-like proteins play in
613 directing diel plant cell regulation.
614

615 **MATERIALS AND METHODS**

616 **Plant Growth and Phenotyping**

617 *Plant Growth* – Wild-type *Arabidopsis thaliana* Col-0 and *rve 4 6 8* seeds were
618 obtained from Dr. Stacy Harmer (University of California - Davis). Seeds were sterilized
619 in 70% (v/v) ethanol for 2 min followed by a 30% (v/v) bleach (Chlorox 7.5%) treatment
620 for 7 min and three washes with distilled water. The seeds were then grown on 0.5x MS
621 media and 7 g/L of agar at pH 5.8 (with KOH). All seeds were cold treated for 3 days at
622 4°C in the dark and exposed to light for a week before being transferred to soil (Sungro,
623 Sunshine Mix® #1). After 21 days of light exposure, entire plants were collected for
624 analysis. Growth chambers were equipped with a programmable Perihelion LED fixture
625 (G2V Optics Inc.) and lined with Reflectix® to ensure a good light diffusion. Plants were
626 grown under a 12h light and 12h dark photoperiod with a temperature of 21°C during the
627 day and 19°C at night. Six LED types (Cree LED XPE, XPE2 XPG families) were used in
628 the fixtures, with characteristic wavelengths of 444 nm, 630 nm, 663 nm, 737 nm, 3000
629 K white, and 6500 K white.

630 *Phenomics measurements* – Each chamber was equipped with a Raspberry Pi 3 B+
631 and an ArduCam Noir Camera (OV5647 1080p) with a motorized IR-CUT filter and two
632 infrared LEDs. Pictures were taken every 15 min over 7 d (between 14 d and 21 d post
633 seed imbibition) and were used to extract plant area and perimeter measurement using
634 PlantCV as previously described (Gehan et al., 2017).

635 *Proteasome inhibitor sensitivity seedling growth experiment* – Col-0 and *rve 4 6 8*
636 seedlings were germinated on 0.5x MS control plates and 0.5x MS plates supplemented
637 with 50 μM MG132 (Millipore Sigma; 474787) and grown under 12:12 photoperiod
638 conditions as described above for 6 days prior to imaging.

639

640 **Starch Iodine Staining and Enzymatic Assay**

641 *Starch Iodine Staining and quantification* – Starch was stained and visualized in
642 *Arabidopsis* rosettes by Lugol's iodine stain. Entire rosettes were decolorized by
643 incubation in 80% ethanol at 80ºC for 30 minutes. Rosettes were rinse 3 times in distilled
644 water and stained 20 min in a 5% (v/v) Lugol's iodine solution (Fisher Scientific). After 3
645 rinses in distilled water, rosettes were washed for an 1h in distilled water to remove the
646 excess of iodine. Rosette leaves were flattened between plastic sheet and excess water
647 removed. Each rosette was analyzed with ImageJ (Abramoff et al 2004;
648 https://imagej.nih.gov/ij/index.html) to record mean values in starch staining pixel intensity
649 as described by Betti et al., (2016).

650 *Starch Extraction and Quantification* – Starch was extracted and assayed as previously
651 described (Smith and Zeeman, 2006). Frozen rosette leaves were ground to a fine
652 powder and homogenized in perchloric acid 8% (Ricca Chemical). The insoluble fraction
653 was pelleted and washed 3 times in ethanol 80% and resuspended in water. Prior
654 quantification, the samples were boiled 15 min at 95ºC to gelatinize the starch and
655 hydrolyzed with α-amylase and amyloglucosidase (Roche) to release the glucose blocks.
656 Glucose content was then measured by spectrophotometry after a 2 enzymes reaction
657 with hexokinase and glucose-6-phosphate dehydrogenase (Roche).

658

659 **RNA isolation and NanoString**

660 Total RNA was isolated and purified using a modified single step TRIzol protocol
661 (Chomczynski and Sacchi, 1987). Plants were flash frozen and homogenized with two
662 glass beads using a Geno/Grinder® for 30s at 1500 x g. Immediately after, 1 mL of TRIzol
663 was added to the sample, and the whole was vortexed and incubated for 10 min at room
664 temperature. The samples were then centrifuged at 13000 x g for 10min to remove
665 extracellular material and glass beads. The supernatant was transferred to a new tube.
666 Subsequently, 200 µL of chloroform was added to the mixture and shaken vigorously by
667 hand for 15 s and the samples were kept for 3 min at room temperature. The samples
668 were centrifuged at 13000 x g for 15 min at 4ºC and the supernatant thus obtained was
669 transferred to a new tube by gentle pipetting, avoiding the interphase slurry. RNA was

670 precipitated by adding 500 µL of 100% isopropanol and the tubes were incubated 10 min
671 at RT and centrifuged at 13000 x g for 10 min at 4ºC. After decanting isopropanol, the
672 pellet was washed with 1 mL of 75% ethanol in nuclease-free water (IDT™) and briefly
673 centrifuged at 7500 x g for 5 min at 4ºC. Total RNA was suspended in nuclease-free water
674 and stored at 80ºC for further use. RNA quantification was performed using a NanoDrop
675 ND 1000 spectrophotometer. The RNA was treated with DNase I, Amp grade (Invitrogen)
676 following the instructions provided by the manufacturer. The purified RNA thus obtained
677 was reverse to cDNA using the RevertAid RT Kit (Thermo Scientific), according to
678 manufacturer's instructions. A minimum of 150ng of purified RNA in 7.5ul was sent to
679 NanoString (NanoString Technologies, Seattle, USA, https://www.nanostring.com) for
680 analysis. The NanoString probes were designed and synthesized by NanoString
681 (Supplementary Data 1). UBC21 (AT5G25760) was used as reference gene.
682
683 **Liquid Chromatography Mass Spectrometry (LC-MS)**
684 *Protein Extraction* - Quick-frozen rosette tissue was ground to a fine powder under
685 liquid N_2 using a mortar and pestle. Ground samples were aliquoted into 400 mg fractions.
686 Aliquoted samples were then extracted at a 1:2 (w/v) ratio with a solution of 50 mM
687 HEPES-KOH pH 8.0, 50 mM NaCl, and 4% (w/v) SDS. Samples were then vortexed and
688 placed in a 95ºC table-top shaking incubator (Eppendorf) at 1100 RPM for 15 mins,
689 followed by an additional 15 mins shaking at room temperature. All samples were then
690 spun at 20,000 x g for 5 min to clarify extractions, with the supernatant retained in fresh
691 1.5 mL Eppendorf tubes. Sample protein concentrations were measured by bicinchoninic
692 acid (BCA) assay (23225; Thermo Scientific). Samples were then reduced with 10 mM
693 dithiothreitol (DTT) at 95ºC for 5 mins, cooled, then alkylated with 30 mM iodoacetamide
694 (IA) for 30 min in the dark without shaking at room temperature. Subsequently, 10 mM
695 DTT was added to each sample, followed by a quick vortex, and incubation for 10 min at
696 room temperature without shaking. Total proteome peptide pools were then generated
697 using a KingFisher Duo (Thermo Scientific) automated sample preparation device as
698 outlined by Leutert et al. (2019) without deviation. Sample digestion was performed using
699 sequencing grade trypsin (V5113; Promega), with generated peptide pools quantified by
700 Nanodrop, normalized to 400 µg for phosphopeptide enrichment and acidified with formic

701 acid (FA) to a final concentration of 5% (v/v) prior to being desalted using 1cc tC18 Sep
702 Pak cartridges (WAT036820; Waters) as previously described (Uhrig et al., 2019).
703 *Phosphopeptide Enrichment* - SepPak eluted peptides were topped up to 65% (v/v)
704 acetonitrile (ACN) and 5% (v/v) trifluoroacetic acid (TFA) prior to enrichment using a
705 KingFisher Duo (Thermo Scientific) automated sample preparation device as outlined by
706 Leutert et al. (2019). We used 500 µg of MagReSyn Ti-IMAC HP matrix (Resyn
707 BioSciences) to enrich phosphorylated peptides. Unbound peptides (total proteome) and
708 phosphopeptides were dried then dissolved in 3% (v/v) ACN / 0.1% (v/v) TFA, desalted
709 using ZipTip C18 pipette tips (ZTC18S960; Millipore) as previously described (Uhrig et
710 al., 2019). All peptides were then dried and re-suspended in 3% (v/v) ACN / 0.1% (v/v)
711 FA immediately prior to MS analysis.
712 *BoxCarDIA Mass Spectrometry* - Changes in the protein abundancies was assessed
713 using trypsin digested samples analysed using a Fusion Lumos Tribrid Orbitrap mass
714 spectrometer (Thermo Scientific) in a data independent acquisition (DIA) mode using the
715 BoxCarDIA method (Mehta et al., 2022). Dissolved peptides (1 µg) were injected using
716 an Easy-nLC 1200 system (LC140; Thermo Scientific) and separated on a 50 cm Easy-
717 Spray PepMap C18 Column (ES803A; Thermo Scientific). A spray voltage of 2.2 kV,
718 funnel RF level of 40 and heated capillary at 300ºC was deployed, with all data acquired
719 in profile mode using positive polarity, with peptide match turned off and isotope exclusion
720 selected. All gradients were run at 300 nL/min with analytical column temperature set to
721 50ºC. Peptides were eluted using a segmented solvent B gradient of 0.1% (v/v) FA in
722 80% (v/v) ACN from 4% - 41% B (0 - 107 min). BoxCar DIA acquisition was performed as
723 previously described (Mehta et al., 2022). MS^1 analysis was performed by using two
724 multiplexed targeted SIM scans of 10 BoxCar windows each, with detection performed at
725 a resolution of 120,000 at 200 m/z and normalized AGC targets of 100% per BoxCar
726 isolation window. Windows were custom designed as previously described (Mehta et al.,
727 2022). An AGC target value for MS^2 fragment spectra was set to 2000%. Twenty-eight
728 38.5 m/z windows were used with an overlap of 1 m/z. Resolution was set to 30,000 using
729 a dynamic maximum injection time and a minimum number of desired points across each
730 peak set to 6.

731 *BoxCarDIA Data Analysis* - All acquired BoxCar DIA data was analyzed in a library-
732 free DIA approach using Spectronaut v14 (Biognosys AG) using default settings. Key
733 search parameters employed include: a protein, peptide and PSM FDR of 1%, trypsin
734 digestion with 1 missed cleavage, fixed modification including carbamidomethylation of
735 cysteine residues and variable modifications including methionine oxidation. Data was
736 Log_2 transformed, globally normalized by median subtraction with significantly changing
737 differentially abundant proteins determined and corrected for multiple comparisons
738 (Bonferroni-corrected *p-value* ≤ 0.05; *q-value ≤ 0.05*).
739 *DDA Mass Spectrometry* - Changes in the protein phosphorylation status was
740 assessed using trypsin digested samples analyzed using a Fusion Lumos Tribrid Orbitrap
741 mass spectrometer in a data dependent acquisition (DDA) mode using the Universal
742 method (Thermo Scientific). Dissolved phosphopeptides were analyzed as described
743 above, using a linear gradient of solvent B (0.1% (v/v) FA in 80% (v/v) ACN): 5% to 22%
744 B, 0 – 110 min; 22% - 35% B, 110 – 120 min; 35 - 95% B, 120 – 125 min at a flow rate of
745 0.3 µl/min at 50°C. Full scan MS1 spectra (350 - 2000 m/z) were acquired with a resolution
746 of 120,000 at 200m/z with a normalized AGC Target of 125% and a maximum injection
747 time of 50 ms. DDA MS2 were acquired in the linear ion trap using quadrupole isolation
748 in a window of 2.5 m/z. Selected ions were HCD fragmented with 35% fragmentation
749 energy, with the ion trap run in rapid scan mode with an AGC target of 200% and a
750 maximum injection time of 100 ms. Precursor ions with a charge state of +2 - +7 and a
751 signal intensity of at least 5.0e3 were selected for fragmentation. All precursor signals
752 selected for MS/MS were dynamically excluded for 30s.
753 *DDA Data Analysis* – All acquired DDA phosphoproteomic data was analyzed using
754 MaxQuant 1.6.14.0 (http://www.maxquant.org/; (Cox and Mann, 2008)) with the following
755 parameters. A protein, peptide and PSM FDR of 1%, trypsin digestion with 1 missed
756 cleavage, fixed modification including carbamidomethylation of cysteine residues and
757 variable modifications including methionine oxidation and phosphorylated serine,
758 threonine and tyrosine. Data was then imported into Perseus version 1.6.14.0 (Tyanova
759 et al., 2016) for further analysis. This involved the removal of reverse hits and
760 contaminants, log_2-transformation, assembly into treatment groups and filtering based on
761 the presence of measured data in at least 2/3 replicates of at least one group. Data were

762 then median normalized, followed by imputation of missing values based on the normal
763 distribution function set to default parameters. All PTM analyses utilized a PTM site
764 localization score threshold ≥ 0.75. Significantly changing differentially abundant
765 phosphopeptides were determined by ANOVA and corrected for multiple comparisons
766 (Benjamini-Hochberg corrected *p-value* ≤ 0.05; *q-value*).
767 All proteomic and phosphoproteomic raw data and search parameters have been
768 uploaded to ProteomeXchange (http://www.proteomexchange.org/) via the Proteomics
769 IDEntification Database (PRIDE; https://www.ebi.ac.uk/pride/). Project Accession:
770 PXD029234.
771
772 **Gas Chromatography Mass Spectrometry (GC-MS)**
773 *Metabolite Extraction and preparation* - Metabolite extraction and preparation was
774 performed with modifications as previously described (Hill and Roessner, 2013; Liu et al.,
775 2016). Tissue was harvested and directly flash frozen in liquid nitrogen. Samples of 100
776 mg (+/- 1 mg) of pulverized tissue were prepared and homogenized in 700 µl of iced-cold
777 methanol (80% v/v). Internal standard 25 µl ribitol at 0.4 $mg.ml^{-1}$ in water. Samples were
778 incubated 2 h at 4°C with shaking and then 15 min at 70°C at 850 rpm in a Thermomixer.
779 Tubes were centrifuged 30 min at 12000 rpm and the supernatants were transferred in
780 new tubes. Polar and non-polar phases were separated by the addition of 700 µl of water
781 and 350 µl of chloroform, then vortexed thoroughly and centrifuged for 15 min at 5000
782 rpm. The upper methanol/ water phase (150 µl) was transferred to a new tube and dried
783 in a vacuum centrifuge at RT. Samples were derivatized with 100 µl of methoxylamine
784 hydrochloride (20 $mg.ml^{-1}$ in pyridine) for 90 min at 30°C at 850 rpm in thermomixer and
785 followed by incubation with 100 µL of N,O-bis(trimethylsilyl)trifluoroacetamide (BSTFA) at
786 80°C during 30 min with shaking at 850 rpm in thermomixer.
787 *GC-MS analysis* - Finally, samples were injected in splitless mode and analyzed using
788 a 7890A gas chromatograph coupled to a 5975C quadrupole mass detector (Agilent
789 Technologies, Palo Alto, CA, USA). In the same manner 1 µl of retention time standard
790 mixture Supelco C7–C40 saturated alkanes standard (1,000 $µg.ml^{-1}$ of each component
791 in hexane) diluted 100 fold (10 $µg.ml^{-1}$ final concentration) was injected and analyzed.
792 Alkanes were dissolved in pyridine at 0.22 $mg.ml^{-1}$ final concentration. Chromatic

793 separation was done with a DB-5MS capillary column (30 m × 0.25 mm × 0.25 µm; Agilent
794 J&W Scientific, Folsom, CA, USA). Inlet temperature was set at 280ºC. Initial GC Oven
795 temperature was set to 80ºC and held for 2 min after injection then GC oven temperature
796 was raised to 300ºC at 7ºC min^{-1}, and finally held at 300ºC for 10 min. Injection and ion
797 source temperatures were adjusted to 300ºC and 200ºC, respectively with a solvent delay
798 of 5 min. The carrier gas (Helium) flow rate was set to 1 $ml.min^{-1}$. The detector was
799 operated in EI mode at 70 eV and in full scan mode (m/z 33–600).
800 *Metabolite identification and quantification* - Compounds were identified by mass
801 spectral and retention time index matching to the mass spectra of the National Institute
802 of Standards and Technology library (NIST20, https://www.nist.gov/) and the Golm
803 Metabolome Database (GMD, http://gmd.mpimp-golm.mpg.de/). Metabolites
804 quantification was performed using MassHunter Software from Agilent. Peaks were
805 integrated and after blank subtraction were normalized by dividing them by the peak area
806 of the internal standard ribitol and by the sample weight.
807
808 **Bioinformatics Analysis and Data Visualization**
809 Visualizations were made using *R* version 3.6.1 and R package *ggplots* in combination
810 with Affinity Designer (https://affinity.serif.com/en-us/designer/; ver. 1.9.1.179). All data
811 was plotted using GraphPad - Prism (ver. 8; https://www.graphpad.com/scientific-
812 software/prism/). Networks were created in Cytoscape (ver 3.7.1; https://cytoscape.org/),
813 using the STRING-DB (https://string-db.org/) and enhancedGrahphics (ver. 1.5.4;
814 https://apps.cytoscape.org/apps/ enhancedgraphics) cytoscape-apps. All association
815 networks were built without data sub-selection and using an edge threshold ≥ 0.7). Gene
816 Ontology Enrichments were performed using TheOntologizer (http://ontologizer.de/)
817 using all identified proteins as the background for enrichment analyses (*q-value* ≤ 0.05),
818 while phosphorylation motif enrichment analysis was performed using Motif-X (Chou and
819 Schwartz, 2011) on the MoMo MEME suite (https://meme-suite.org/meme/) as previously
820 described (Mehta et al., 2021). Subcellular localization information for proteins was
821 obtained from SUBA4 (https://suba.live/).
822
823 **Proteasome activity assay**

824 Proteasome activity was measured using the fluorogenic substrate N-Succinyl-Leu-
825 Leu-Val-Tyr-7-Amido-4-Methylcoumarin (Millipore Sigma; S6510) as described Üstün et
826 al. (2017). Briefly, 100 µg of rosette tissue of 3 week old plants was extracted with 250
827 µL of extraction buffer (2 mM ATP, 50 mM HEPES-KOH (adjusted to pH 7.2 with 1 N
828 KOH); 2 mM DTT; 0.25 M sucrose). After clarifying by centrifugation at 18,000 g for 15
829 minutes, total protein content in the extracts was quantified with a Bradford assay (Bio-
830 Rad; 5000006). The assay was performed using 50 µg of total protein extract and 300
831 µM of substrate in assay buffer (100mM HEPES-KOH pH 7.8, 5mM $MgCl_2$, 10 mM KCl,
832 and 2 mM ATP) at 30°C. Fluorescence was measured at 1.5 minute intervals with an
833 excitation at 360nm and emission wavelength at 460nm for a period of 2 hours after an
834 initial 2 hour incubation. Activity was reported as Relative Fluorescence Units/min based
835 on the slope of the linear portion of the emission curve (MeanV in the Gen5 software).
836

837 **ACKNOWLEDGEMENTS**

838 The authors would like to thank Dr. Stacey Harmer for providing *rve 4 6 8* and
839 corresponding WT Col-0 seeds as well as Dr. Pascal Schläpfer for assistance with the
840 MoMo MEME suite. We would also like to thank G2V Optics Inc. for providing their LED
841 lighting system. As well, we would like to thank Jack Moore of the Alberta Mass
842 Spectrometry and Proteomics Facility as well as Broderick Wood, Jacob Blazusiak and
843 Mohamad Jamaleddine of the University of Alberta Faculty of Science Research IT team
844 for their technical assistance.
845

846 **FUNDING**

847 This work was funded by the National Science and Engineering Research Council of
848 Canada (NSERC), Mathematics of Information Technology and Complex Systems
849 (MITACS), Alberta Innovates Campus Alberta Small Business Engagement (AI-CASBE)
850 and the Canadian Foundation for Innovation (CFI).
851

852 **LITERATURE CITED**

853 **Aarabi F, Naake T, Fernie AR, Hoefgen R** (2020) Coordinating Sulfur Pools under Sulfate
854 Deprivation. Trends Plant Sci **25:** 1227-1239

855 **Abramoff MD, Magalhaes PJ, and Ram SJ** (2004) Image Processing with ImageJ. Biophotonics
856 International. **11:** 36-42
857 **Akten B, Jauch E, Genova GK, Kim EY, Edery I, Raabe T, Jackson FR** (2003) A role for CK2
858 in the Drosophila circadian oscillator. Nat Neurosci **6:** 251-257
859 **Artus NN, Uemura M, Steponkus PL, Gilmour SJ, Lin C, Thomashow MF** (1996) Constitutive
860 expression of the cold-regulated Arabidopsis thaliana COR15a gene affects both
861 chloroplast and protoplast freezing tolerance. Proc Natl Acad Sci U S A **93**: 13404-9
862 **Astot C, Dolezal K, Nordstrom A, Wang Q, Kunkel T, Moritz T, Chua NH, Sandberg G** (2000)
863 An alternative cytokinin biosynthesis pathway. Proc Natl Acad Sci U S A **97:** 14778-14783
864 **Baerenfaller K, Massonnet C, Walsh S, Baginsky S, Buhlmann P, Hennig L, Hirsch-**
865 **Hoffmann M, Howell KA, Kahlau S, Radziejwoski A, Russenberger D, Rutishauser**
866 **D, Small I, Stekhoven D, Sulpice R, Svozil J, Wuyts N, Stitt M, Hilson P, Granier C,**
867 **Gruissem W** (2012) Systems-based analysis of Arabidopsis leaf growth reveals
868 adaptation to water deficit. Mol Syst Biol **8:** 606
869 **Barbier FF, Cao D, Fichtner F, Weiste C, Perez-Garcia MD, Caradeuc M, Le Gourrierec J,**
870 **Sakr S, Beveridge CA** (2021) HEXOKINASE1 signalling promotes shoot branching and
871 interacts with cytokinin and strigolactone pathways. New Phytol **231:** 1088-1104
872 **Betti C, Vanhoutte I, Coutuer S, De Rycke R, Mishev K, Vuylsteke M, Aesaert S, Rombaut**
873 **D, Gallardo R, De Smet F, Xu J, Van Lijsebettens M, Van Breusegem F, Inzé D,**
874 **Rousseau F, Schymkowitz J, Russinova E** (2016) Sequence-Specific Protein
875 Aggregation Generates Defined Protein Knockdowns in Plants. Plant Physiol. **171**: 773-
876 87
877 **Bognar LK, Hall A, Adam E, Thain SC, Nagy F, Millar AJ** (1999) The circadian clock controls
878 the expression pattern of the circadian input photoreceptor, phytochrome B. Proc Natl
879 Acad Sci U S A **96:** 14652-14657
880 **Cervela-Cardona L, Yoshida T, Zhang Y, Okada M, Fernie A, Mas P** (2021) Circadian Control
881 of Metabolism by the Clock Component TOC1. Front Plant Sci **12:** 683516
882 **Chew YH, Seaton DD, Mengin V, Flis A, Mugford ST, Smith AM, Stitt M, Millar AJ** (2017)
883 Linking circadian time to growth rate quantitatively via carbon metabolism. BioRxIv
884 **Chomczynski P, Sacchi N** (1987) Single-step method of RNA isolation by acid guanidinium
885 thiocyanate-phenol-chloroform extraction. Anal Biochem **162:** 156-159
886 **Chou MF, Schwartz D** (2011) Biological sequence motif discovery using motif-x. Curr Protoc
887 Bioinformatics **Chapter 13:** Unit 13 15-24
888 **Choudhary MK, Nomura Y, Shi H, Nakagami H, Somers DE** (2016) Circadian
889 profiling of the Arabidopsis proteome using 2D-DIGE. Front. Plant Sci. 7: 1007
890 **Choudhary MK, Nomura Y, Wang L, Nakagami H, Somers DE** (2015) Quantitative
891 circadian phosphoproteomic analysis of Arabidopsis reveals extensive clock
892 control of key components in physiological, metabolic and signaling pathways.
893 Mol. Cell. Proteom. 14: 2243-2260
894 **Covington MF, Maloof JN, Straume M, Kay SA, Harmer SL** (2008) Global transcriptome
895 analysis reveals circadian regulation of key pathways in plant growth and development.
896 Genome Biol **9:** R130
897 **Cox J, Mann M** (2008) MaxQuant enables high peptide identification rates, individualized p.p.b.-
898 range mass accuracies and proteome-wide protein quantification. Nat Biotechnol **26:**
899 1367-1372
900 **Creux N, Harmer S** (2019) Circadian Rhythms in Plants. Cold Spring Harb Perspect Biol **11**
901 **Critchley JH, Zeeman SC, Takaha T, Smith AM, Smith SM** (2001) A critical role for
902 disproportionating enzyme in starch breakdown is revealed by a knock-out mutation in
903 Arabidopsis. Plant J. **26:** 89-100

904 **Devlin PF, Kay SA** (2000) Cryptochromes are required for phytochrome signaling to the circadian
905 clock but not for rhythmicity. Plant Cell **12:** 2499-2510
906 **Farinas B, Mas P** (2011) Functional implication of the MYB transcription factor RVE8/LCL5 in the
907 circadian control of histone acetylation. Plant J **66:** 318-329
908 **Feke A, Liu W, Hong J, Li MW, Lee CM, Zhou EK, Gendron JM** (2019) Decoys provide a
909 scalable platform for the identification of plant E3 ubiquitin ligases that regulate circadian
910 function. Elife **8**
911 **Feke AM, Hong J, Liu W, Gendron JM** (2020) A Decoy Library Uncovers U-Box E3 Ubiquitin
912 Ligases That Regulate Flowering Time in Arabidopsis. Genetics **215:** 699-712
913 **Flis A, Mengin V, Ivakov AA, Mugford ST, Hubberten HM, Encke B, Krohn N, Hohne M, Feil**
914 **R, Hoefgen R, Lunn JE, Millar AJ, Smith AM, Sulpice R, Stitt M** (2019) Multiple
915 circadian clock outputs regulate diel turnover of carbon and nitrogen reserves. Plant Cell
916 Environ **42:** 549-573
917 **Flis A, Sulpice R, Seaton DD, Ivakov AA, Liput M, Abel C, Millar AJ, Stitt M** (2016)
918 Photoperiod-dependent changes in the phase of core clock transcripts and global
919 transcriptional outputs at dawn and dusk in Arabidopsis. Plant Cell Environ **39:** 1955-1981
920 **Fukushima A, Kusano M, Nakamichi N, Kobayashi M, Hayashi N, Sakakibara H, Mizuno T,**
921 **Saito K** (2009) Impact of clock-associated Arabidopsis pseudo-response regulators in
922 metabolic coordination. Proc Natl Acad Sci U S A **106:** 7251-7256
923 **Gehan MA, Fahlgren N, Abbasi A, Berry JC, Callen ST, Chavez L, Doust AN, Feldman MJ,**
924 **Gilbert KB, Hodge JG, Hoyer JS, Lin A, Liu S, Lizarraga C, Lorence A, Miller M,**
925 **Platon E, Tessman M, Sax T** (2017) PlantCV v2: Image analysis software for high-
926 throughput plant phenotyping. PeerJ **5:** e4088
927 **Gibson S, Arondel V, Iba K, Somerville C** (1994) Cloning of a temperature-regulated gene
928 encoding a chloroplast omega-3 desaturase from Arabidopsis thaliana. Plant Physiol **106:**
929 1615-1621
930 **Gladman N P, Marshall R S, Lee K-H, Vierstra R D** (2016), The Proteasome Stress Regulon Is
931 Controlled by a Pair of NAC Transcription Factors in Arabidopsis, The Plant Cell, Volume
932 28, Issue 6, Pages 1279–1296, https://doi.org/10.1105/tpc.15.01022
933 **Graf A, Coman D, Uhrig RG, Walsh S, Flis A, Stitt M, Gruissem W** (2017) Parallel analysis of
934 Arabidopsis circadian clock mutants reveals different scales of transcriptome and
935 proteome regulation. Open Biol **7**
936 **Gray JA, Shalit-Kaneh A, Chu DN, Hsu PY, Harmer SL** (2017) The REVEILLE Clock Genes
937 Inhibit Growth of Juvenile and Adult Plants by Control of Cell Size. Plant Physiol **173:**
938 2308-2322
939 **Greenham K, McClung CR** (2015) Integrating circadian dynamics with physiological processes
940 in plants. Nat Rev Genet **16:** 598-610
941 **Han J-J, Yan X, Wang Q, Tang L, Yu F, Huang X, Wang, Y, Liu J-X, Xie Q** (2019), The β5
942 subunit is essential for intact 26S proteasome assembly to specifically promote plant
943 autotrophic growth under salt stress. New Phytol, 221: 1359-1368.
944 https://doi.org/10.1111/nph.15471
945 **Hardtke CS, Okamoto H, Stoop-Myer C, Deng XW** (2002) Biochemical evidence for ubiquitin
946 ligase activity of the Arabidopsis COP1 interacting protein 8 (CIP8). Plant J **30:** 385-394
947 **He M, Ding NZ** (2020) Plant Unsaturated Fatty Acids: Multiple Roles in Stress Response. Front
948 Plant Sci **11:** 562785
949 **Heazlewood JL, Durek P, Hummel J, Selbig J, Weckwerth W, Walther D, Schulze WX** (2008)
950 PhosPhAt: a database of phosphorylation sites in Arabidopsis thaliana and a plant-specific
951 phosphorylation site predictor. Nucleic Acids Res **36:** D1015-1021
952 **Heazlewood JL, Tonti-Filippini JS, Gout AM, Day DA, Whelan J, Millar AH** (2004)
953 Experimental analysis of the Arabidopsis mitochondrial proteome highlights signaling and

954 regulatory components, provides assessment of targeting prediction programs, and
955 indicates plant-specific mitochondrial proteins. Plant Cell **16:** 241-256
956 **Hei S, Liu Z, Huang A, She X** (2018) The regulator of G-protein signalling protein mediates D-
957 glucose-induced stomatal closure via triggering hydrogen peroxide and nitric oxide
958 production in Arabidopsis. Funct Plant Biol **45:** 509-518
959 **Herold A, Lewis DH** (1977) MANNOSE AND GREEN PLANTS: OCCURRENCE, PHYSIOLOGY
960 AND METABOLISM, AND USE AS A TOOL TO STUDY THE ROLE OF
961 ORTHOPHOSPHATE. New Phytologist **79:** 1-40
962 **Hill CB, Roessner U** (2013) Metabolic Profiling of Plants by GC–MS. The Handbook of Plant
963 Metabolomics
964 **Hsu PY, Devisetty UK, Harmer SL** (2013) Accurate timekeeping is controlled by a cycling
965 activator in Arabidopsis. Elife **2:** e00473
966 **Huang S, Li L, Petereit J, Millar AH** (2020) Protein turnover rates in plant mitochondria.
967 Mitochondrion **53:** 57-65
968 **Huang X, Zhang X, Gong Z, Yang S, Shi Y** (2017) ABI4 represses the expression of type-A
969 ARRs to inhibit seed germination in Arabidopsis. Plant J **89:** 354-365
970 **Jaglo-Ottosen KR, Gilmour SJ, Zarka DG, Schabenberger O, Thomashow MF** (1998)
971 Arabidopsis CBF1 overexpression induces COR genes and enhances freezing tolerance.
972 Science **280**: 104-6.
973 **Kidokoro S, Hayashi K, Haraguchi H, Ishikawa T, Soma F, Konoura I, Toda S, Mizoi J,**
974 **Suzuki T, Shinozaki K, Yamaguchi-Shinozaki K** (2021) Posttranslational regulation of
975 multiple clock-related transcription factors triggers cold-inducible gene expression in
976 Arabidopsis. Proc Natl Acad Sci U S A **118:** e2021048118
977 **Kotchoni SO, Larrimore KE, Mukherjee M, Kempinski CF, Barth C** (2009) Alterations in the
978 endogenous ascorbic acid content affect flowering time in Arabidopsis. Plant Physiol **149:**
979 803-815
980 **Krahmer J, Hindle M, Perby LK, Nielson TH, VanOoijen G, Halliday KJ, Le Bihan T, Millar**
981 **AJ** (2022) Circadian protein regulation in the green lineage II. The clock gene circuit
982 controls a phospho-dawn in Arabidopsis thaliana. Mol. Cell. Proteom **21:** 100172
983 **Kurepa J, Wang S, Li Y, Zaitlin D, Pierce JA, Smalle JA** (2009) Loss of 26S Proteasome
984 Function Leads to Increased Cell Size and Decreased Cell Number in Arabidopsis Shoot
985 Organs. Plant Physiology **150 :** 178-189
986 **Kurepa J, Wang S, Li Y, Smalle JA** (2009) Proteasome regulation, plant growth and stress
987 tolerance. Plant Signalling and Behaviour **4:** 924-927
988 **Lee SH, Li CW, Koh KW, Chuang HY, Chen YR, Lin CS, Chan MT** (2014) MSRB7 reverses
989 oxidation of GSTF2/3 to confer tolerance of Arabidopsis thaliana to oxidative stress. J Exp
990 Bot **65:** 5049-5062
991 **Leschevin M, Ismael M, Quero A, San Clemente H, Roulard R, Bassard S, Marcelo P,**
992 **Pageau K, Jamet E, Rayon C** (2021) Physiological and Biochemical Traits of Two Major
993 Arabidopsis Accessions, Col-0 and Ws, Under Salinity. Front Plant Sci **12:** 639154
994 **Leutert M, Rodriguez-Mias RA, Fukuda NK, Villen J** (2019) R2-P2 rapid-robotic
995 phosphoproteomics enables multidimensional cell signaling studies. Mol Syst Biol **15:**
996 e9021
997 **Li L, Nelson CJ, Trosch J, Castleden I, Huang S, Millar AH** (2017) Protein Degradation Rate
998 in Arabidopsis thaliana Leaf Growth and Development. Plant Cell **29:** 207-228
999 **Liu XS, Yang X, Wang LM, Duan QQ, Huang DF** (2016) Comparative analysis of metabolites
1000 profile in spinach (Spinacia oleracea L.) affected by different concentrations of gly and
1001 nitrate. Scientia Horticulturae **204:** 8-15
1002 **Lu H, McClung CR, Zhang C** (2017) Tick Tock: Circadian Regulation of Plant Innate Immunity.
1003 Annu Rev Phytopathol **55:** 287-311

1004 **Lu SX, Liu H, Knowles SM, Li J, Ma L, Tobin EM, Lin C** (2011) A role for protein kinase casein
1005 kinase2 alpha-subunits in the Arabidopsis circadian clock. Plant Physiol **157:** 1537-1545
1006 **Marti Ruiz MC, Jung HJ, Webb AAR** (2020) Circadian gating of dark-induced increases in
1007 chloroplast- and cytosolic-free calcium in Arabidopsis. New Phytol **225:** 1993-2005
1008 **Maszkowska, J, Dębski, J, Kulik, A, et al.** (2019) Phosphoproteomic analysis reveals that dehydrins
1009 ERD10 and ERD14 are phosphorylated by SNF1-related protein kinase 2.10 in response to
1010 osmotic stress. *Plant Cell Environ*. **42:** 931– 946
1011 **McClung CR** (2019) The Plant Circadian Oscillator. Biology (Basel) **8:** 14
1012 **Mehlmer N, Wurzinger B, Stael S, Hofmann-Rodrigues D, Csaszar E, Pfister B, Bayer R,**
1013 **Teige M** (2010) The Ca(2+) -dependent protein kinase CPK3 is required for MAPK-
1014 independent salt-stress acclimation in Arabidopsis. Plant J **63:** 484-498
1015 **Mehta D, Ghahremani M, Perez-Fernandez M, Tan M, Schlapfer P, Plaxton WC, Uhrig RG**
1016 (2021) Phosphate and phosphite have a differential impact on the proteome and
1017 phosphoproteome of Arabidopsis suspension cell cultures. Plant J **105:** 924-941
1018 **Mehta D, Krahmer J, Uhrig RG** (2021) Closing the protein gap in plant chronobiology. Plant J
1019 **106:** 1509-1522
1020 **Mehta D, Scandola S, Uhrig RG** (2022) BoxCar and Library-Free Data-Independent Acquisition
1021 Substantially Improve the Depth, Range, and Completeness of Label-Free Quantitative
1022 Proteomics. Anal Chem **94:** 793–802
1023 **Mori IC, Murata Y, Yang Y, Munemasa S, Wang YF, Andreoli S, Tiriac H, Alonso JM, Harper**
1024 **JF, Ecker JR, Kwak JM, Schroeder JI** (2006) CDPKs CPK6 and CPK3 function in ABA
1025 regulation of guard cell S-type anion- and Ca(2+)-permeable channels and stomatal
1026 closure. PLoS Biol **4:** e327
1027 **Mulekar JJ, Huq E** (2014) Expanding roles of protein kinase CK2 in regulating plant growth and
1028 development. J Exp Bot **65:** 2883-2893
1029 **Nakamichi N** (2020) The Transcriptional Network in the Arabidopsis Circadian Clock System.
1030 Genes (Basel) **11**
1031 **Nohales MA, Kay SA** (2016) Molecular mechanisms at the core of the plant circadian oscillator.
1032 Nat Struct Mol Biol **23:** 1061-1069
1033 **Patterson JA, Tetlow IJ, Emes MJ** (2018) Bioinformatic and in vitro Analyses of Arabidopsis
1034 Starch Synthase 2 Reveal Post-translational Regulatory Mechanisms. Front Plant Sci **9:**
1035 1338
1036 **Purzner T, Purzner J, Buckstaff T, Cozza G, Gholamin S, Rusert JM, Hartl TA, Sanders J,**
1037 **Conley N, Ge X, Langan M, Ramaswamy V, Ellis L, Litzenburger U, Bolin S,**
1038 **Theruvath J, Nitta R, Qi L, Li XN, Li G, Taylor MD, Wechsler-Reya RJ, Pinna LA, Cho**
1039 **YJ, Fuller MT, Elias JE, Scott MP** (2018) Developmental phosphoproteomics identifies
1040 the kinase CK2 as a driver of Hedgehog signaling and a therapeutic target in
1041 medulloblastoma. Sci Signal **11:** eaau5147
1042 **Qi T, Liu Z, Fan M, Chen Y, Tian H, Wu D, Gao H, Ren C, Song S, Xie D** (2017) GDP-D-
1043 mannose epimerase regulates male gametophyte development, plant growth and leaf
1044 senescence in Arabidopsis. Sci Rep **7:** 10309
1045 **Qin N, Xu D, Li J, Deng XW** (2020) COP9 signalosome: Discovery, conservation, activity and,
1046 function. JIPB **62:** 90-103
1047 **Rawat R, Takahashi N, Hsu PY, Jones MA, Schwartz J, Salemi MR, Phinney BS, Harmer SL**
1048 (2011) REVEILLE8 and PSEUDO-REPONSE REGULATOR5 form a negative feedback
1049 loop within the Arabidopsis circadian clock. PLoS Genet **7:** e1001350
1050 **Rodriguez MC, Mehta D, Tan M, Uhrig RG** (2021) Quantitative Proteome and PTMome Analysis
1051 of Arabidopsis thaliana Root Responses to Persistent Osmotic and Salinity Stress. Plant
1052 Cell Physiol **62:** 1012-1029

1053 **Ruiz-Sola MA, Barja MV, Manzano D, Llorente B, Schipper B, Beekwilder J, Rodriguez-**
1054 **Concepcion M** (2016) A Single Arabidopsis Gene Encodes Two Differentially Targeted
1055 Geranylgeranyl Diphosphate Synthase Isoforms. Plant Physiol **172:** 1393-1402
1056 **Sadandom A, Bailey M, Ewan R, Lee J, Neils S** (2012) The ubiquitin-proteasome system:
1057 central modifier of plant signalling. New Phytologist **196:** 13-28.
1058 **Sanchez SE, Rugnone ML, Kay SA** (2020) Light Perception: A Matter of Time. Mol Plant **13:**
1059 363-385
1060 **Senkler J, Senkler M, Eubel H, Hildebrandt T, Lengwenus C, Schertl P, Schwarzlander M,**
1061 **Wagner S, Wittig I, Braun HP** (2017) The mitochondrial complexome of Arabidopsis
1062 thaliana. Plant J **89:** 1079-1092
1063 **Seok HY, Nguyen LV, Van Nguyen D, Lee SY, Moon YH** (2020) Investigation of a Novel Salt
1064 Stress-Responsive Pathway Mediated by Arabidopsis DEAD-Box RNA Helicase Gene
1065 AtRH17 Using RNA-Seq Analysis. Int J Mol Sci **21:** 1595
1066 **Sharma V, Ichikawa M, Freeze HH** (2014) Mannose metabolism: more than meets the eye.
1067 Biochem Biophys Res Commun **453:** 220-228
1068 **Shim JS, Kubota A, Imaizumi T** (2017) Circadian Clock and Photoperiodic Flowering in
1069 Arabidopsis: CONSTANS Is a Hub for Signal Integration. Plant Physiol **173:** 5-15
1070 **Simon NML, Graham CA, Comben NE, Hetherington AM, Dodd AN** (2020) The Circadian
1071 Clock Influences the Long-Term Water Use Efficiency of Arabidopsis. Plant Physiol **183:**
1072 317-330
1073 **Smalle J, Kurepa J, Yang P, Babiychuk E, Kushnir S, Durski A, Vierstra R D** (2002) Cytokinin
1074 Growth Responses in Arabidopsis Involve the 26S Proteasome Subunit RPN12. The Plant
1075 Cell, **14** 1: 17-32
1076 **Smith AM, Zeeman SC** (2006) Quantification of starch in plant tissues. Nature Protocols **1:** 1342-
1077 1345
1078 **Smith AM, Zeeman SC** (2020) Starch: A Flexible, Adaptable Carbon Store Coupled to Plant
1079 Growth. Annu Rev Plant Biol **71:** 217-245
1080 **Somers DE, Devlin PF, Kay SA** (1998) Phytochromes and cryptochromes in the entrainment of
1081 the Arabidopsis circadian clock. Science **282:** 1488-1490
1082 **Streb S, Zeeman SC** (2012) Starch metabolism in Arabidopsis. Arabidopsis Book **10:** e0160
1083 **Sugano S, Andronis C, Green RM, Wang ZY, Tobin EM** (1998) Protein kinase CK2 interacts
1084 with and phosphorylates the Arabidopsis circadian clock-associated 1 protein. Proc Natl
1085 Acad Sci U S A **95:** 11020-11025
1086 **Tamaru T, Hirayama J, Isojima Y, Nagai K, Norioka S, Takamatsu K, Sassone-Corsi P** (2009)
1087 CK2alpha phosphorylates BMAL1 to regulate the mammalian clock. Nat Struct Mol Biol
1088 **16:** 446-448
1089 **Tetlow IJ, Wait R, Lu Z, Akkasaeng R, Bowsher CG, Esposito S, Kosar-Hashemi B, Morell**
1090 **MK, Emes MJ** (2004) Protein phosphorylation in amyloplasts regulates starch branching
1091 enzyme activity and protein-protein interactions. Plant Cell **16:** 694-708
1092 **Thalmann M, Pazmino D, Seung D, Horrer D, Nigro A, Meier T, Kolling K, Pfeifhofer HW,**
1093 **Zeeman SC, Santelia D** (2016) Regulation of Leaf Starch Degradation by Abscisic Acid
1094 Is Important for Osmotic Stress Tolerance in Plants. Plant Cell **28:** 1860-1878
1095 **Toledo M, Batista-Gonzalez A, Merheb E, Aoun ML, Tarabra E, Feng D, Sarparanta J, Merlo**
1096 **P, Botre F, Schwartz GJ, Pessin JE, Singh R** (2018) Autophagy Regulates the Liver
1097 Clock and Glucose Metabolism by Degrading CRY1. Cell Metab **28:** 268-281 e264
1098 **Torres-Franklin ML, Repellin A, Huynh VB, d'Arcy-Lameta A, Zuily-Fodil Y, Thi ATP** (2009)
1099 Omega-3 fatty acid desaturase (FAD3, FAD7, FAD8) gene expression and linolenic acid
1100 content in cowpea leaves submitted to drought and after rehydration. Environmental and
1101 Experimental Botany **65:** 162-169

1102 **Tyanova S, Temu T, Sinitcyn P, Carlson A, Hein MY, Geiger T, Mann M, Cox J** (2016) The
1103 Perseus computational platform for comprehensive analysis of (prote)omics data. Nat
1104 Methods **13:** 731-740
1105 **Uehara TN, Mizutani Y, Kuwata K, Hirota T, Sato A, Mizoi J, Takao S, Matsuo H, Suzuki T,**
1106 **Ito S, Saito AN, Nishiwaki-Ohkawa T, Yamaguchi-Shinozaki K, Yoshimura T, Kay SA,**
1107 **Itami K, Kinoshita T, Yamaguchi J, Nakamichi N** (2019) Casein kinase 1 family
1108 regulates PRR5 and TOC1 in the Arabidopsis circadian clock. Proc Natl Acad Sci U S A
1109 **116:** 11528-11536
1110 **Uhrig RG, Echevarria-Zomeno S, Schlapfer P, Grossmann J, Roschitzki B, Koerber N,**
1111 **Fiorani F, Gruissem W** (2021) Diurnal dynamics of the Arabidopsis rosette proteome and
1112 phosphoproteome. Plant Cell Environ **44:** 821-841
1113 **Uhrig RG, Schlapfer P, Roschitzki B, Hirsch-Hoffmann M, Gruissem W** (2019) Diurnal
1114 changes in concerted plant protein phosphorylation and acetylation in Arabidopsis organs
1115 and seedlings. Plant J **99:** 176-194
1116 **Upchurch RG** (2008) Fatty acid unsaturation, mobilization, and regulation in the response of
1117 plants to stress. Biotechnol Lett **30:** 967-977
1118 **Usmani MM, Nawaz F, Majeed S, Shehzad MA, Ahmad KS, Akhtar G, Aqib M, Shabbir RN**
1119 (2020) Sulfate-mediated Drought Tolerance in Maize Involves Regulation at Physiological
1120 and Biochemical Levels. Sci Rep **10:** 1147
1121 **Üstün, S. and Börnke, F. (2017).** Ubiquitin Proteasome Activity Measurement in Total Plant
1122 Extracts. Bio-protocol 7(17): e2532.
1123 **Veremeichik GN, Shkryl YN, Gorpenchenko TY, Silantieva SA, Avramenko TV,**
1124 **Brodovskaya EV, Bulgakov VP** (2021) Inactivation of the auto-inhibitory domain in
1125 Arabidopsis AtCPK1 leads to increased salt, cold and heat tolerance in the AtCPK1-
1126 transformed Rubia cordifolia L cell cultures. Plant Physiol Biochem **159:** 372-382
1127 **Wang W, Paik I, Kim J, Hou X, Sung S, Huq E** (2021) Direct phosphorylation of HY5 by SPA
1128 kinases to regulate photomorphogenesis in Arabidopsis. New Phytol **230:** 2311-2326
1129 **Wasternack C, Hause B** (2019) The missing link in jasmonic acid biosynthesis. Nat Plants **5:**
1130 776-777
1131 **Zhang M, Barg R, Yin M, Gueta-Dahan Y, Leikin-Frenkel A, Salts Y, Shabtai S, Ben-Hayyim**
1132 **G** (2005) Modulated fatty acid desaturation via overexpression of two distinct omega-3
1133 desaturases differentially alters tolerance to various abiotic stresses in transgenic tobacco
1134 cells and plants. Plant J **44:** 361-371
1135 **Zhu W, Zhou H, Lin F, Zhao X, Jiang Y, Xu D, Deng XW** (2020) COLD-REGULATED GENE27
1136 Integrates Signals from Light and the Circadian Clock to Promote Hypocotyl Growth in
1137 Arabidopsis. Plant Cell **32:** 3155-3169

1138 **Zhu, Y., Huang, P., Guo, P., Chong, L., Yu, G., Sun, X., Hu, T., Li, Y., Hsu, C.-C., Tang, K.,**
1139 **Zhou, Y., Zhao, C., Gao, W., Tao, W.A., Mengiste, T. and Zhu, J.-K.** (2020), CDK8 is
1140 associated with RAP2.6 and SnRK2.6 and positively modulates abscisic acid signaling
1141 and drought response in Arabidopsis. New Phytol, **228:** 1573-1590.

1142

1143 **TABLE CAPTIONS**

1144 **Table I: Quantified and significantly changing proteome and phosphoproteome.**

1145 Protein groups and peptides are shown (n=4; *q-value* ≤ 0.05; fold-change (FC) ≥ 1.5).

1146

1147 **FIGURE CAPTIONS**

1148 **Figure 1: Phenotypic analysis of *rve 4 6 8* plant growth and development. (A)** Iodine
1149 starch staining of rosettes at 28 d post-imbibition. (**B**) Enzymatic quantification of starch
1150 levels in rosettes. All phenotyping was conducted under a 12 h : 12 h light : dark
1151 photoperiod using 100 µmol m-2 s-1 light. Stars denote Bonferroni adjusted *p-value*
1152 significance: (***) *p-value* ≤ 0.005 and (*) *p-value* ≤ 0.05. **(C)** Starch related genes PGM1,
1153 GBSS1 and SEX4. All time-points and genotypes were analyzed in biological triplicate
1154 (n=3). Stars denote Student's t-test *p-value* significance: (***) *p-value* ≤ 0.005, (**) *p-value*
1155 ≤ 0.01 and (*) *p-value* ≤ 0.05. Primer pairs used in the nanostring analysis are described
1156 in Supplemental Data 1.
1157
1158 **Figure 2: Diel mRNA gene expression analysis of circadian clock and**
1159 **photoreceptor related genes in *rve 4 6 8* and Col-0 plants.** Select genes from different
1160 circadian / diel implicated plant cell processes were examined for their expression level
1161 at end-of-night (ZT0) and end-of-day (ZT12) by NanoString expression analysis (see
1162 Materials and Methods). **(A)** Expression of circadian clock / RVE8-like related genes
1163 *CCA1*, *LHY*, *TOC1*, *PRR5*, *ELF4*, *PIF4* and *PIF5*. **(B)** Expression of photoreceptors *PhyA*,
1164 *PhyB*, *CRY1*, *PHOT1*, *PHOT2* and *ZTL*. All time-points and genotypes were analyzed in
1165 biological triplicate (n=3). Stars denote Student's t-test *p-value* significance: (***) *p-value*
1166 ≤ 0.005, (**) *p-value* ≤ 0.01 and (*) *p-value* ≤ 0.05. Primer pairs used in the nanostring
1167 analysis are described in Supplemental Data 1.
1168
1169 **Figure 3: Analysis of the quantified proteome and phosphoproteome changes at**
1170 **ZT0 or ZT12 in *rve 4 6 8* versus Col-0.** The significantly changing **(A)** proteome and **(B)**
1171 phosphoproteome (n=4; fold-change ≥ 1.5, *q-value* ≤ 0.05) were plotted by venn diagram
1172 and scatterplot to visualize the overlap and Log_2 fold-change (Log_2FC) between *rve 4 6*
1173 *8* and WT Col-0 plants at ZT0 and ZT12. Gene ontology (GO) enrichment of biological
1174 processes, subcellular localization and molecular function was then performed to
1175 systemically contextualize proteome and phosphoproteme changes (see Materials and
1176 Methods).
1177

1178 **Figure 4: Association network analysis of significant genotypic proteome**
1179 **fluctuations at ZT0 and ZT12.** The association network depicts significant Log_2FC in
1180 protein abundance between *rve 4 6 8* and WT Col-0 at ZT0 and ZT12 (*q-value* ≤ 0.05;
1181 Supplemental Data 2). Networks were generated using Cytoscape and a combination of
1182 the STRING-DB and enhancedGraphics App (see Materials and Methods) using all
1183 datatypes and an edge score ≥ 0.7. Nodes with no edges ≥ 0.7 were removed. Brighter
1184 red (*rve 4 6 8*) or blue (WT Col-0) coloration indicates the relative increase in measured
1185 Log_2FC protein abundance in that corresponding genotype. Highlighted node clusters
1186 were manually annotated using a combination of ThaleMine
1187 (https://bar.utoronto.ca/thalemine/begin.do), TAIR (https://www.arabidopsis.org/) and
1188 Cytoscape Functional Annotation.
1189
1190 **Figure 5: Association network analysis of significant genotypic phosphoproteome**
1191 **fluctuations at ZT0 and ZT12.** The association network depicts significant median
1192 Log_2FC phosphoproteome changes between *rve 4 6 8* and WT Col-0 at ZT0 and ZT12
1193 (*q-value* ≤ 0.05; Supplemental Data 3). Networks were generated using Cytoscape and a
1194 combination of the STRING-DB and enhancedGraphics App (see materials and methods)
1195 using all datatypes and an edge score ≥ 0.7. Nodes with no edges ≥ 0.7 or only edges ≤
1196 0.6 were removed. Brighter red (*rve 4 6 8*) or blue (WT Col-0) coloration indicates the
1197 relative increase in measured Log_2FC protein abundance in that corresponding genotype.
1198 Highlighted node clusters were manually annotated using a combination of ThaleMine
1199 (https://bar.utoronto.ca/thalemine/begin.do), TAIR (https://www.arabidopsis.org/) and
1200 Cytoscape Functional Annotation.
1201
1202 **Figure 6: Relative Log_2FC fold-change change in diel metabolite levels.** Rosette
1203 tissue (28 d post-imbibition) was sampled at ZT0, ZT6, ZT12 and ZT18 as outlined in the
1204 Materials and Methods. Brighter red (*rve 4 6 8*) or blue (WT Col-0) coloration indicates
1205 the relative increase in measured Log_2FC metabolite abundance in that corresponding
1206 genotype.
1207

1208 **Figure 7: Proteasome function is reduced in *rve 4 6 8*. (A)** Proteasome activity in
1209 relative fluorescence units per minute (RFU/min) measured in crude extracts of three
1210 week old *rve 4 6 8* and WT Col-0 plants. (**** Bonferroni adjusted *p-value* <0.0001; *
1211 Bonferroni adjusted *p-value* < 0.05) (**B**) Seedling growth experiments with proteasome
1212 inhibitor treatment (50 µM MG132). Seedlings were germinated, stratified, and then grown
1213 for 6 d under 12:12 LD conditions. A total of six replicate plates per condition were
1214 assayed (Additional plates depicted in Supplemental Figure 4).
1215
1216 **SUPPLEMENTAL FIGURES**
1217 **Supplemental Figure 1. Confirmation of known *rve 4 6 8* phenotypes.** Phenomics
1218 experimentation was designed to parallel that resolved by previously by Gray *et al.,* 2017
1219 to ensure growth conditions produced comparable phenotypes prior to molecular
1220 experimentation. **(A & B)** Rosette area (mm^2) and perimeter (mm) over 5 d of growth (15
1221 d – 19 d post-imbibition). Data was extracted using PlantCV (n=20). **(C & D)** Rosette fresh
1222 and dry weight (mg) at 28 d post-imbibition (n=10). **(E)** Days to bolting (n=20). Stars
1223 denote Student's t-test *p-value* significance: (***) *p-value* ≤ 0.005 and (*) *p-value* ≤ 0.05.
1224
1225 **Supplemental Figure 2: Diel mRNA gene expression analysis of circadian clock and**
1226 **phytohormone related genes in *rve 4 6 8* and Col-0 plants.** Select genes from different
1227 circadian / diel implicated plant cell processes were examined for their expression level
1228 at ZT0 and ZT12 by quantitative NanoString expression analysis (see Materials and
1229 Methods). **(A)** Expression of circadian clock / RVE8-like related genes *RVE4*, *RVE8*,
1230 *PRR7*, *GI* and *CO*. **(B)** Expression of phytohormone genes *GGPPS1*, *ARR7* and *IAA4*.
1231 All time-points and genotypes analyzed in biological triplicate (n=3). Stars denote
1232 Student's t-test *p-value* significance: (***) *p-value* ≤ 0.005, (**) *p-value* ≤ 0.01 and (*) *p-*
1233 *value* ≤ 0.05. Primer pairs used in the nanostring analysis are described in Supplemental
1234 Data 1.
1235
1236 **Supplemental Figure 3. Association network analysis of significantly changing**
1237 **phosphoproteins maintaining an enriched protein kinase motifs.** The
1238 phopshopeptides corresponding to one or more of the 5 enriched phosphorylation motifs

1239 were used to generate an association network that relates protein kinase motifs to the
1240 underlying protein networks which exhibit genotypic changes in phosphorylation
1241 (Supplemental Data 5). Networks were generated using Cytoscape and a combination of
1242 the STRING-DB and enhancedGraphics App (see Materials and Methods) using all
1243 datatypes and an edge score ≥ 0.7. Protein localization was determined using SUBA4
1244 (https://suba.live/). Highlighted node clusters were manually annotated using a
1245 combination of ThaleMine (https://bar.utoronto.ca/thalemine/begin.do) and TAIR
1246 (https://www.arabidopsis.org/).
1247
1248 **Supplemental Figure 4:** Additional replicates for the proteasome inhibitor sensitivity
1249 growth assay described in Figure 7B.
1250
1251 **SUPPLEMENTAL DATA**
1252 **Supplemental Data 1: Primer sets used in Nanostring analysis.**
1253 **Supplemental Data 2: All quantified and significantly changing proteome data.**
1254 **Supplemental Data 3: All quantified and significantly changing phosphoproteome**
1255 **data.**
1256 **Supplemental Data 4: Gene Ontology enrichment analysis.**
1257 **Supplemental Data 5: Comparative analysis of significantly changing**
1258 **phosphorylation sites to significantly cycling**
1259 **phosphorylation sites (JTK-cycle *p-value* ≤ 0.05).**
1260 **Supplemental Data 6: Diel changes in proteasome.**
1261 **Supplemental Data 7: MotifX phosphor-motif enrichment analysis using MoMo**
1262 **MEME suite.**
1263 **Supplemental Data 8: Gas Chromatography Mass Spectrometry (GC-MS) data**
1264
1265

Table I

	Quantified		*Significantly Changing	
	Protein Groups	Peptides	Protein Groups	Peptides
Proteome	3934	n/a	536	n/a
Phosphoproteome	1137	1872	346	425

* (n=4; *q-value* ≤ 0.05; FC ≥ 1.5)

Figure 1

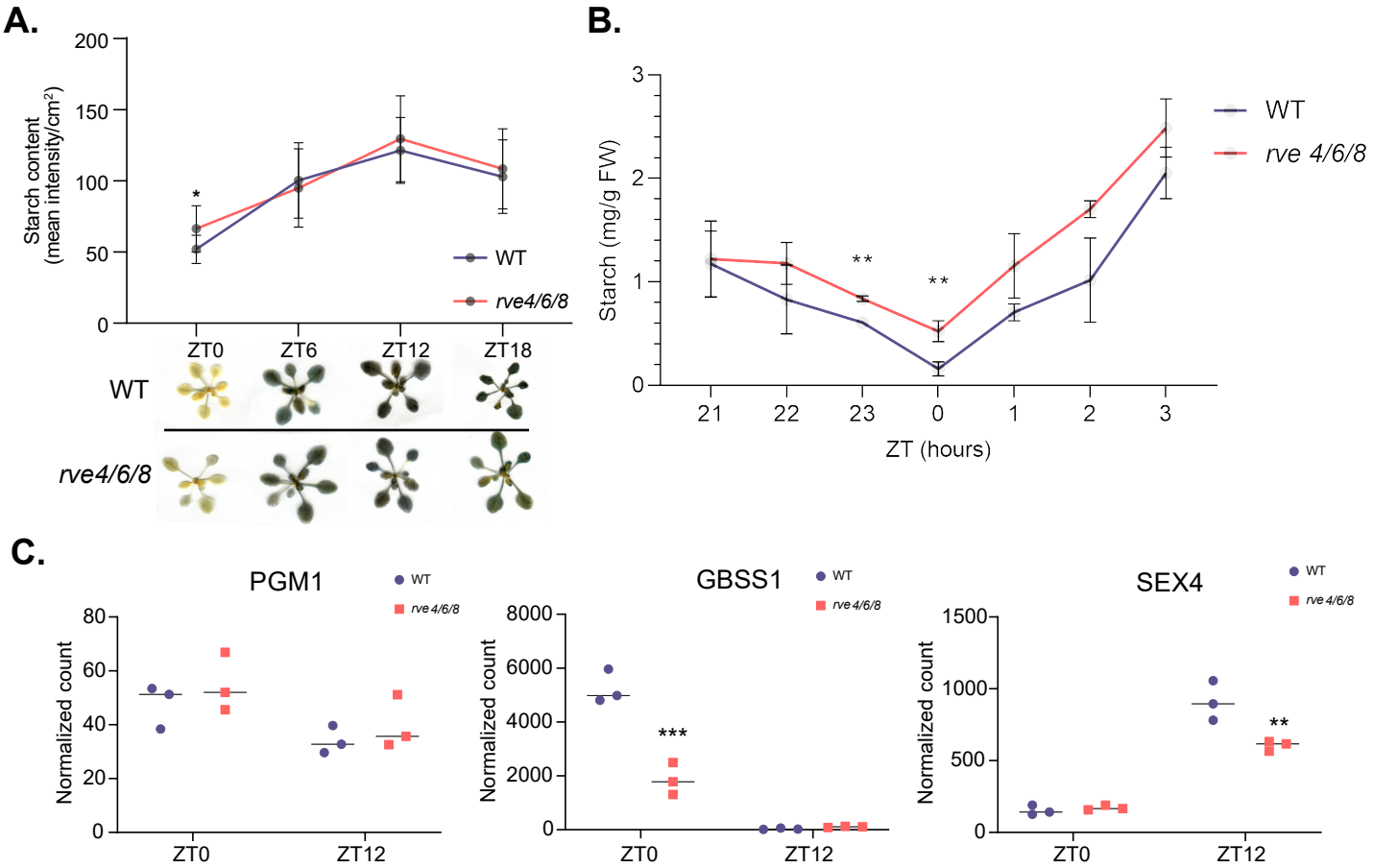
A.
Starch content (mean intensity/cm²)
200
150
100
50
0
*
WT
rve4/6/8
ZT0
ZT6
ZT12
ZT18
WT
rve4/6/8
B.
Starch (mg/g FW)
3
2
1
0
**
**
WT
rve 4/6/8
21
22
23
0
1
2
3
ZT (hours)
C.
PGM1
GBSS1
SEX4
WT
rve 4/6/8
Normalized count
80
60
40
20
0
8000
6000
4000
2000
1500
1000
500
***
**
ZT0
ZT12

Figure 2

A. Circadian Clock / RVE8-Like Related

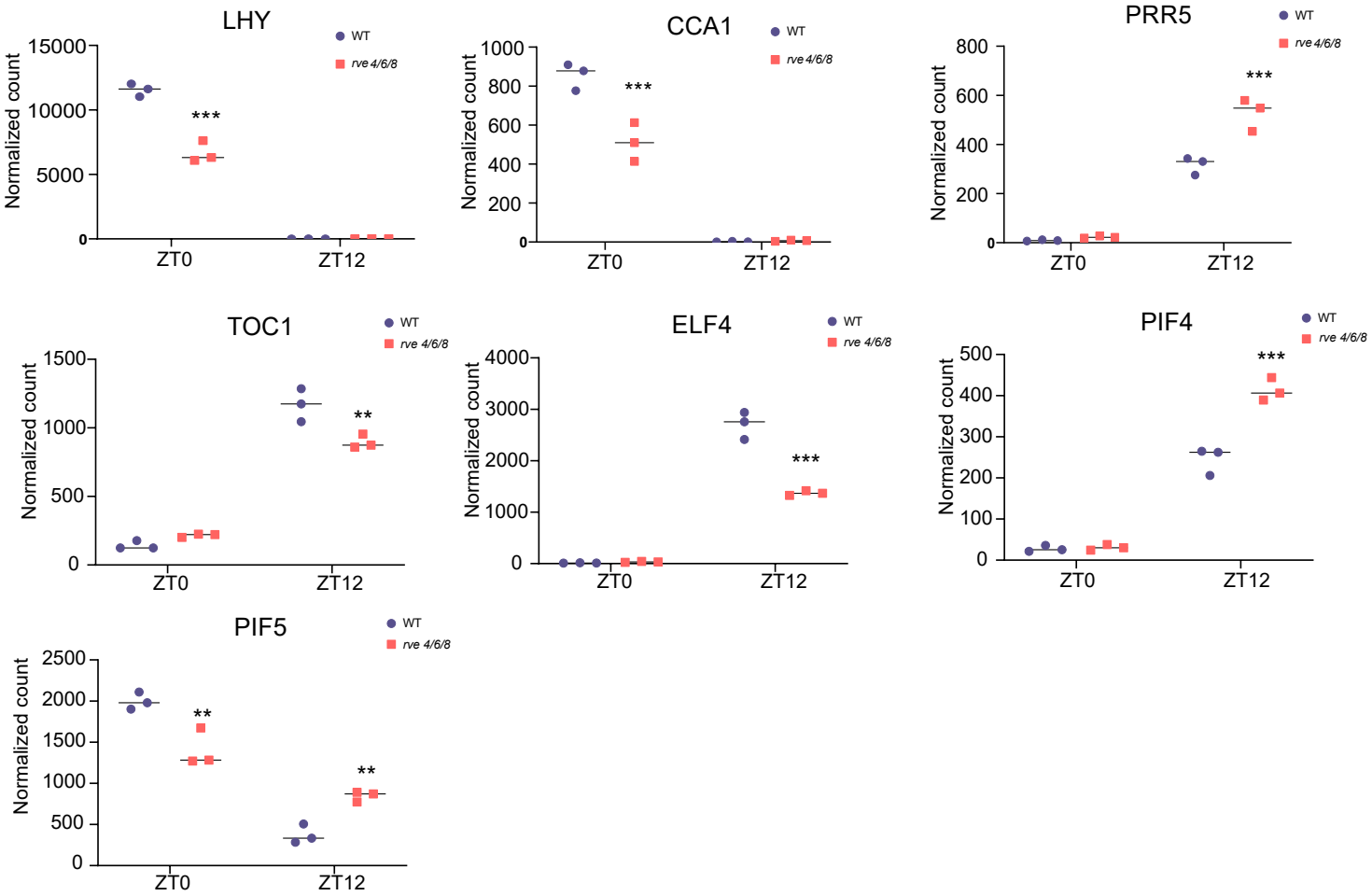

B. Photoreceptors

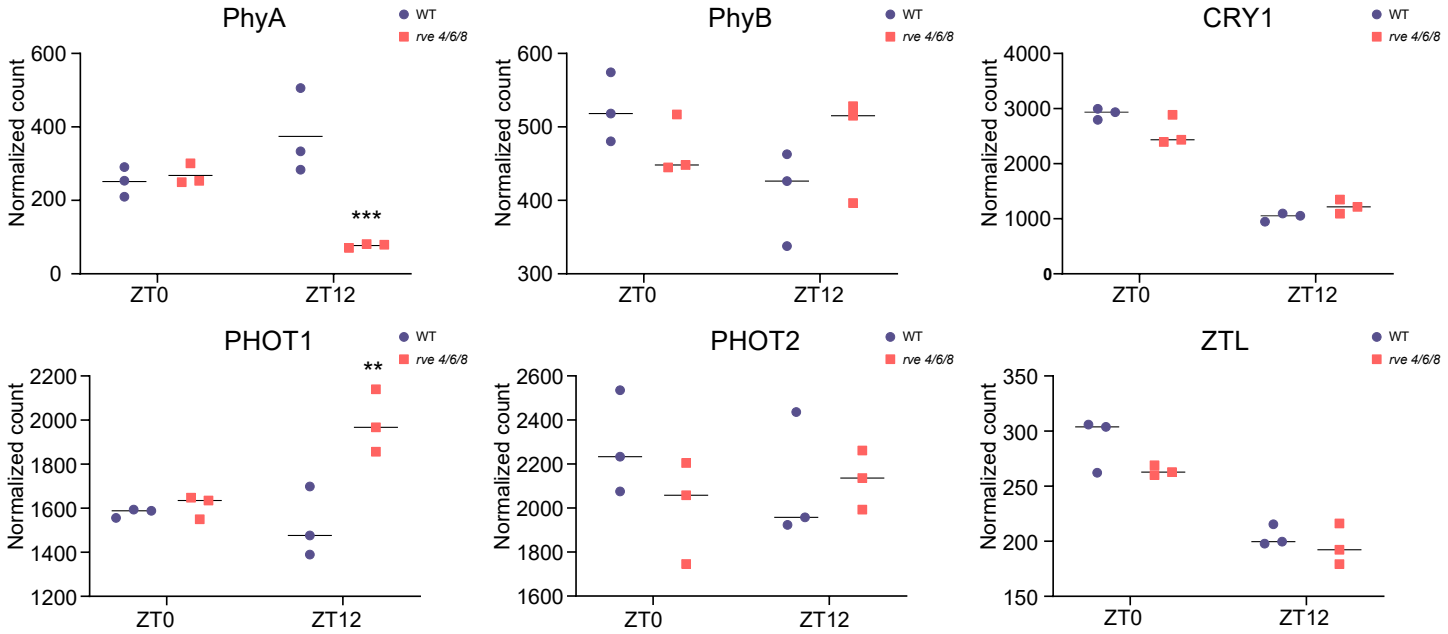

Figure 3

A.

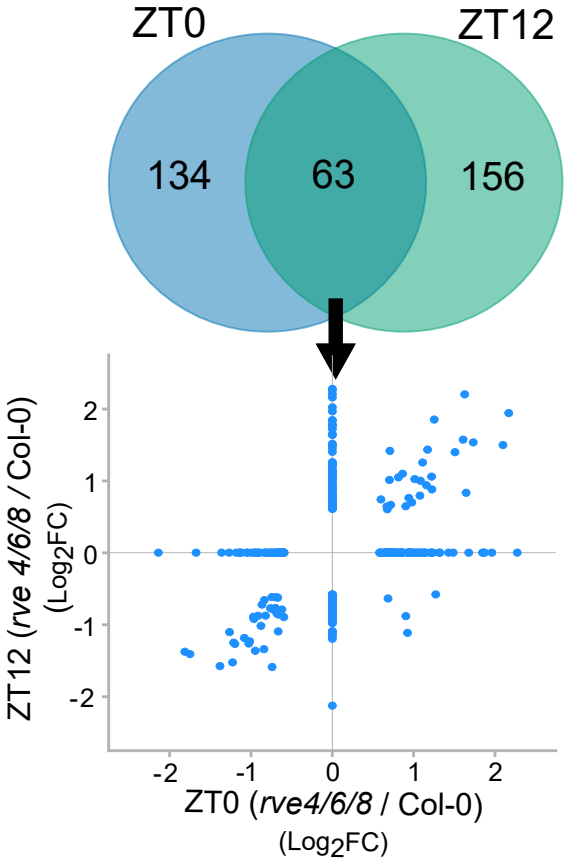

Gene Ontology Enrichment

Biological Processes:
- Macromolecule catabolism
- Cellular catabolic processes
- Response to acid chemical
- Protein catabolic processes
- Proteolysis
- Polysaccharide metabolism

Subcellular Location:
- Proteasome core complex
- Peptidase complex
- Proteasome complex
- Cytoplasm

Molecular Function:
- Threonine-type peptidase activity
- Pattern binding
- Carbohydrate binding
- Phosphotransferase activity

B.

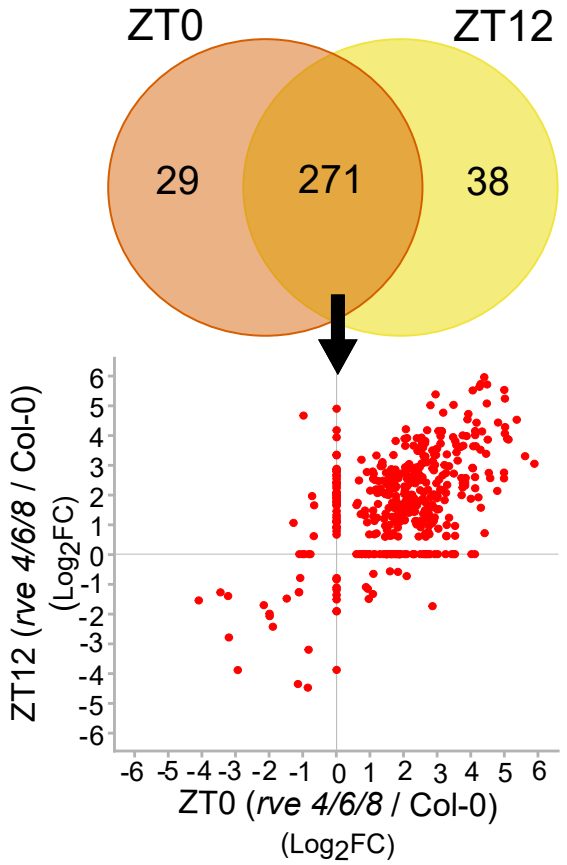

Gene Ontology Enrichment

Biological Processes:
- Macromolecule metabolism
- Response to alcohol
- Organelle organization
- Response to abscisic acid
- Cell cycle
- Cell division
- Response to acid chemical
- Response to lipid
- Chromosome segregation

Subcellular Location:
- Nucleus
- Cytoplasm
- Plasma membrane

Molecular Function:
- Hydrolase activity
- Transferase activity

Figure 4

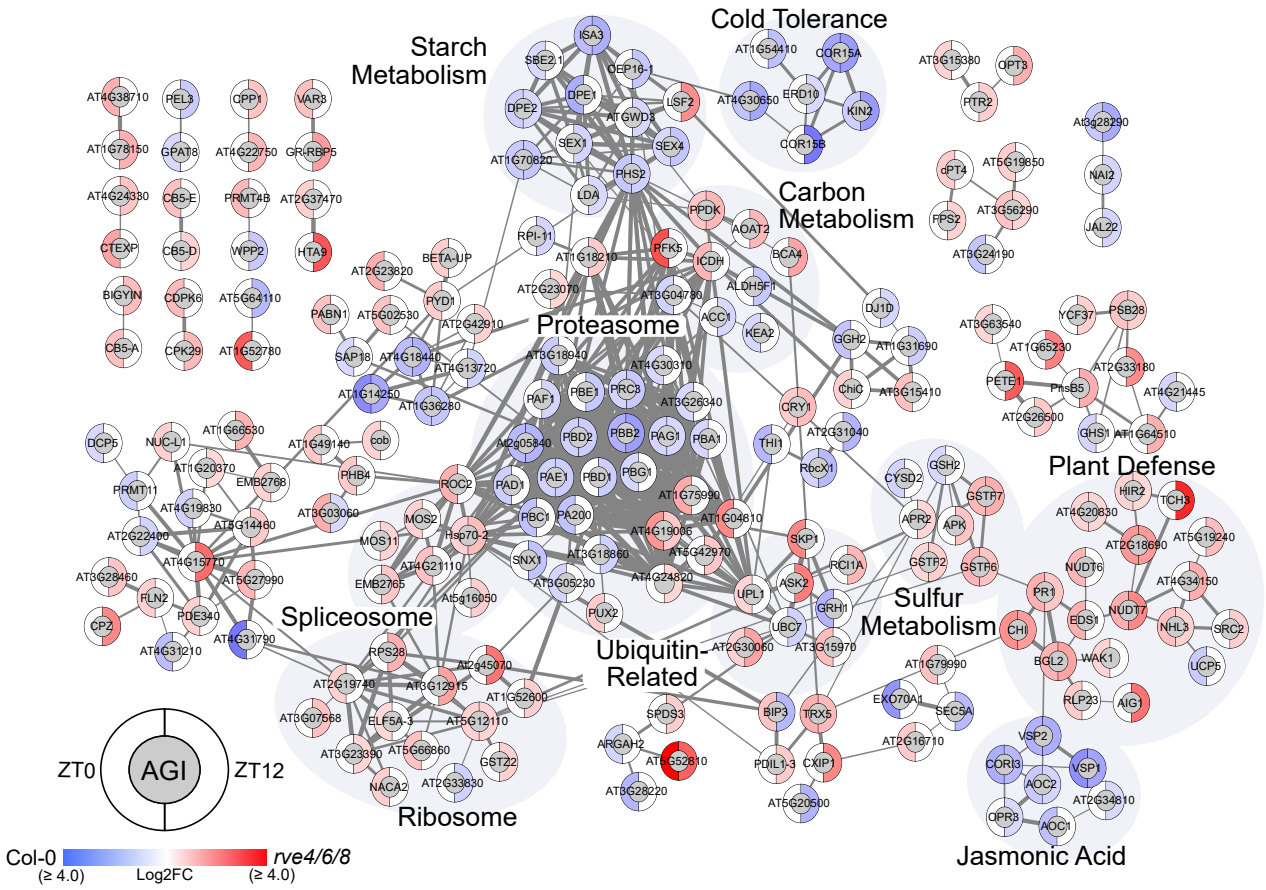
Starch Metabolism
Cold Tolerance
Carbon Metabolism
Proteasome
Plant Defense
Spliceosome
Ubiquitin-Related
Sulfur Metabolism
Ribosome
Jasmonic Acid
ZT0
AGI
ZT12
Col-0
(≥ 4.0)
Log2FC
rve4/6/8
(≥ 4.0)

Figure 5

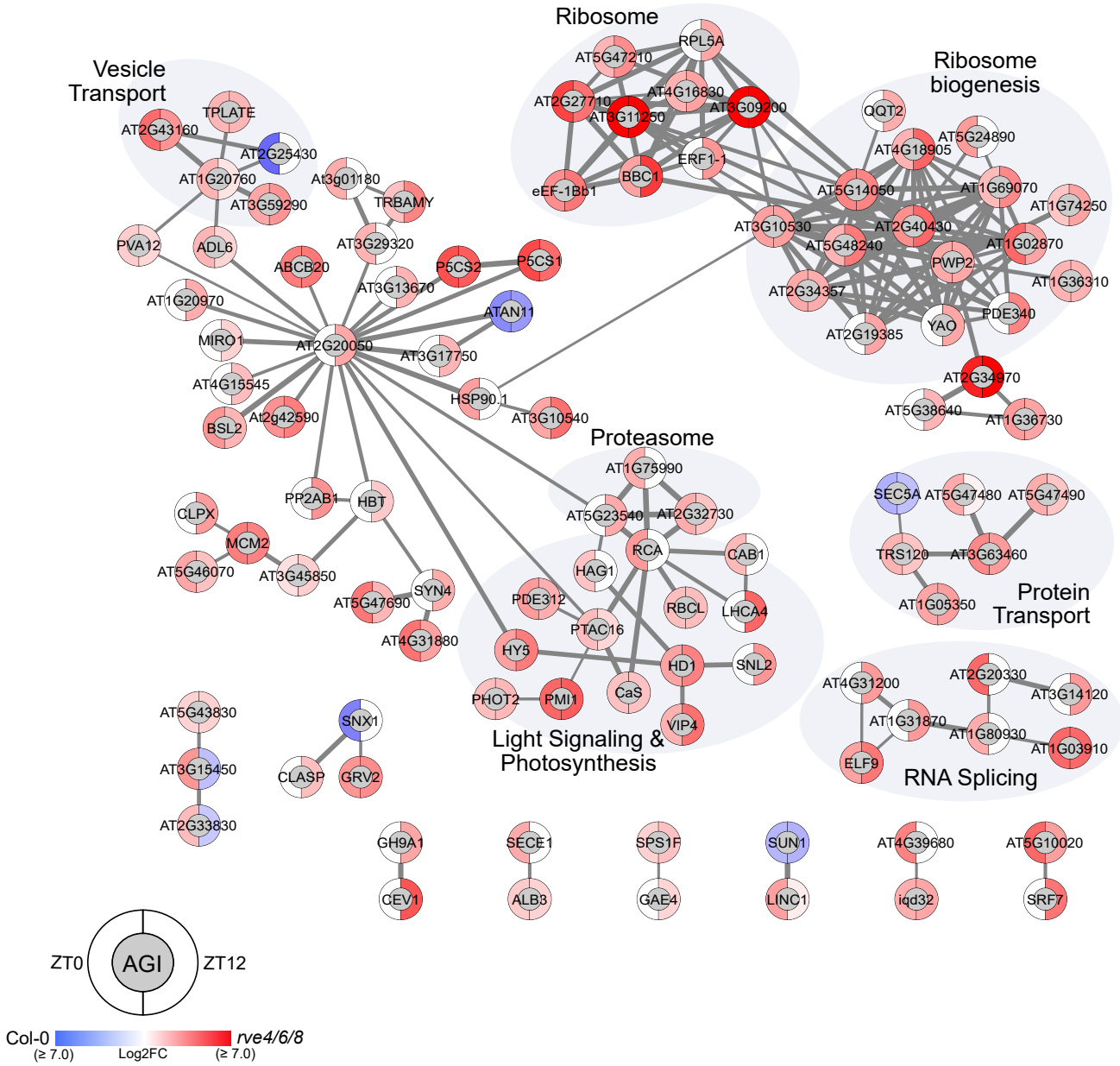
Ribosome
RPL5A
AT5G47210
AT4G16830
AT2G27710
AT3G11250
AT3G09200
ERF1-1
BBC1
eEF-1Bb1
Ribosome biogenesis
QQT2
AT5G24890
AT4G18905
AT5G14050
AT1G69070
AT1G74250
AT3G10530
AT2G40430
AT5G48240
AT1G02870
PWP2
AT1G36310
AT2G34357
YAO
PDE340
AT2G19385
AT2G34970
AT5G38640
AT1G36730
Vesicle Transport
TPLATE
AT2G43160
AT2G25430
AT1G20760
AT3G59290
At3g01180
TRBAMY
PVA12
ADL6
AT3G29320
ABCB20
P5CS2
P5CS1
AT3G13670
AT1G20970
ATAN11
MIRO1
AT2G20050
AT3G17750
AT4G15545
HSP90.1
AT3G10540
BSL2
At2g42590
Proteasome
AT1G75990
AT5G23540
AT2G32730
RCA
CAB1
HAG1
RBCL
LHCA4
PDE312
PTAC16
HY5
HD1
SNL2
PHOT2
PMI1
CaS
VIP4
Light Signaling & Photosynthesis
SEC5A
AT5G47480
AT5G47490
TRS120
AT3G63460
AT1G05350
Protein Transport
PP2AB1
HBT
CLPX
MCM2
AT5G46070
AT3G45850
SYN4
AT5G47690
AT4G31880
AT4G31200
AT2G20330
AT3G14120
AT1G31870
AT1G80930
AT1G03910
ELF9
RNA Splicing
AT5G43830
AT3G15450
AT2G33830
SNX1
CLASP
GRV2
GH9A1
CEV1
SECE1
ALB3
SPS1F
GAE4
SUN1
LINC1
AT4G39680
iqd32
AT5G10020
SRF7
ZT0
AGI
ZT12
Col-0
rve4/6/8
(≥ 7.0)
Log2FC
(≥ 7.0)

Figure 6

	Metabolite	zt0	zt6	zt12	zt18
AMINO ACIDS	Proline	0.11876	-0.3251	0.14782	-0.0452
	Glycine	0.33635	-0.1793	0.07189	0.00667
	Alanine	0.42136	-0.0392	-0.3874	0.06209
	Valine	0.17249	-0.3952	-0.2908	-0.0968
	Serine	-0.0516	-0.668	-0.3435	-0.2243
	Threonine	-0.2489	-0.7273	-0.4982	-0.6009
	Oxoproline	0.76778	0.28482	0.37774	0.5045
	Glutamic acid	0.90973	0.34547	0.43199	0.56407
	Phenylalanine	1.37177	-0.0823	-0.4578	-0.2088
	Asparagine	0.04382	0.53934	-0.5256	0.41541
ORGANIC ACID	Shikimic acid	0.73752	0.20973	0.35809	0.45792
	Citric acid	0.22559	-0.0101	-0.0188	0.02254
	Malic acid	0.27184	-0.1122	0.14143	0.3441
	Sinapinic acid	0.65492	0.29656	0.37613	0.52211
	Succinic acid	0.29573	0.15162	0.44533	0.52778
	Glyceric acid	0.29827	1.3348	1.68119	0.82126
	Fumaric acid	1.50538	0.69384	1.05776	1.42337
FA	Stearic acid	0.07598	-0.0329	0.18202	0.42968
	α-Linolenic acid	1.79841	0.60266	0.11563	0.57337
	Palmitic acid	0.18004	0.01183	0.17715	0.28635
SUGARS	Ribose	0.426	0.08479	0.39341	0.26825
	Glucopyranoside	0.9053	0.29352	0.47691	0.52401
	Sucrose	0.92758	-0.0673	-0.2546	-0.1345
	Fructose	-0.1311	0.58635	0.29415	-0.171
	Glucose	-0.2645	0.12747	0.11925	-0.7815
	Mannose	0.01893	2.86785	1.69011	1.82642
	Mannopyranose	0.426	2.92767	1.6949	1.71009
	Galactose	0.33122	-0.4348	-0.2996	-0.2505
OTHER	Myo-inositol	0.75642	-0.0377	0.49368	0.45784
	Glycerol	-0.1105	-0.1713	0.16128	-0.1205
	Phytol	0.64536	-1.0376	-0.6581	-0.9052

Figure 7

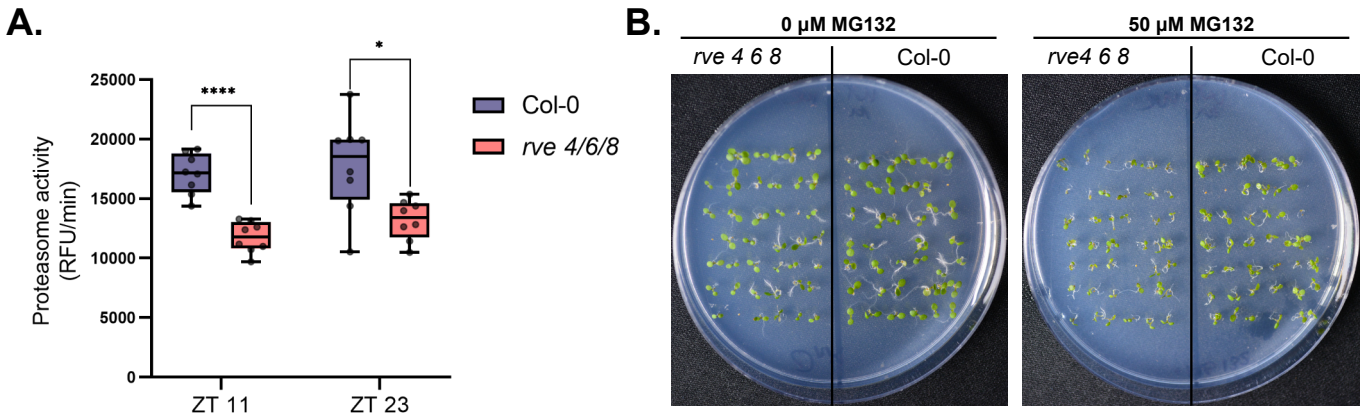
A.
Proteasome activity (RFU/min)
25000
20000
15000
10000
5000
0
****
*
ZT 11
ZT 23
Col-0
rve 4/6/8
B.
0 µM MG132
50 µM MG132
rve 4 6 8
Col-0
rve4 6 8
Col-0